ministerie van verkeer en waterstaat

koninklijk nederlands meteorologisch instituut

Vertical profiles of the structure parameter of refractive index and the structure parameter of temperature in the earth's atmosphere

J.W.M. Cuijpers

wetenschappelijke rapporten WR 87-13

scientific reports WR 87-13

de bilt 1987

KNMI

Vertical profiles of the structure parameter of refractive index and the structure parameter of temperature in the earth's atmosphere

Hans Cuijpers
(Universiteit van Amsterdam)

KNMI, De Bilt
December 1987

Contents

Voorwoord

In het kader van het groot-onderzoek, dat dient te leiden tot een afstudeerverslag, ben ik als stagiair bij het KNMI werkzaam geweest. Ik heb daar met behulp van metingen en literatuurgegevens de mate van turbulentie in verschillende delen van de aardatmosfeer onderzocht. Hiermee kan worden bekeken waar in de atmosfeer verstoringen van sterbeeldjes ontstaan, die tijdens waarnemingen met telescopen worden gezien. De resultaten van dat onderzoek zijn in dit verslag weergegeven.

Tijdens het onderzoek ben ik op problemen gestuit, die ik niet makkelijk zelf kon oplossen. Ik heb daarbij echter een beroep kunnen doen op verschillende medewerkers van het KNMI. Hulp van en discussies met hen hebben mij veel geholpen tijdens het onderzoek. Daarvoor wil ik ze hierbij hartelijk bedanken.

Met name wil ik Wim Kohsiek bedanken, die mij tijdens de gehele periode heeft begeleid en aan het eind dit verslag kritisch heeft doorgelezen.

Ook Peter Duynkerke, die met zijn computermodel profielen van de temperatuur structuur parameter in de nachtelijke grenslaag heeft berekend en deel I. van dit verslag van nuttige opmerkingen heeft voorzien, wil ik bedanken.

Tenslotte wil ik Sandra Klutz en de medewerkers van de tekenkamer bedanken voor hun bijdrage aan het tot stand komen van dit verslag.

Hans Cuijpers

Abstract

Vertical profiles of the structure parameter of temperature C_T^2 in the stable, nocturnal boundary layer are obtained with the models described by Nieuwstadt (1984, 1985), Sorbjan (1986) and Duynkerke and Driedonks (1987). These theoretical profiles are compared with observed profiles obtained at the meteorological mast at Cabauw, The Netherlands. From the observations it is found that C_T^2 is large in the surface layer and small at the top of the boundary layer. Observations during nights with moderate geostrophic winds or during the first few hours of nights with a high geostrophic wind show a continuous decrease of C_T^2 from surface layer to the top of the boundary layer. Observations done later at nights with a high geostrophic wind show the development of a maximum of C_T^2 at about three quarters of the boundary layer. From the comparison with the models we conclude that the observed profiles are most satisfactory described by the model of Duynkerke and Driedonks.

In part II., the influence of turbulence in the earth's atmosphere on stellar image degradation is discussed. By measuring temperature fluctuations or stellar scintillations the vertical profiles of the structure parameter of refractive index C_N^2 can be obtained. Observations show that C_N^2 varies from position to position and from time to time. In the first 100-200 m above the ground C_N^2 is large. Above the boundary layer C_N^2 decreases sharply. In the troposphere turbulence is layered. C_N^2 generally decreases with height. However, an increase is seen in situations with winds from or towards mountains or near temperature inversions. In the stratosphere C_N^2 is small. We conclude that the lower troposphere is most responsible for phase fluctuations causing image movement and image blurring, whereas the tropopause region seems to be more responsible for amplitude fluctuations causing scintillation.

General Introduction

While observing with their ground-based telescopes astronomers are confronted with the influence of the earth's atmosphere on stellar image quality. Variations in brightness or sharpness or jumping of the image can be observed.

These disturbances are caused by turbulence in the atmosphere. Due to turbulence the refractive index of air changes. These local changes cause small deviations about the mean path of a beam of starlight and two neighbouring beams which have slightly different mean paths will encounter slightly different deviations. After passing through a turbulent layer, the two beams will tend to converge or to diverge. As the light finally reaches the telescope it has experienced changes in amplitude and phase.

To investigate the disturbing work of the atmosphere on stellar images one needs information about the vertical profiles of the varying refractive index of air. As a measure of the intensity of the turbulent refractive index the structure parameter of refractive index is used. A larger value indicates more refractive index fluctuations, which are associated with more turbulent mixing of air.

This study deals with the vertical profiles of the structure parameter of refractive index and the structure parameter of temperature, which is at optical wavelengths closely related to the first one. The whole study is divided into two parts. In part I. we will discuss the vertical profiles of the temperature structure parameter in the stable, nocturnal boundary layer. It is based on measurements conducted at the meteorological mast at Cabauw, The Netherlands. The theory of structure parameters is given. Measurements and the results of model calculations are discussed.

In part II., that is based on a literature study, we will discuss vertical profiles of the refractive index structure parameter. The theory of the effects of atmospheric turbulence on seeing is given.

Part I.

Vertical profiles of the structure parameter of temperature in the stable, nocturnal boundary layer

1. Introduction

The behaviour of the structure parameter of temperature in the mixed layer, that is the part of the convective boundary layer for which $-z/L >> 1$ holds (L is the Monin-Obukhov length and z the height above the surface), has been rather well documented (e.g., Wyngaard and LeMone, 1980; Fairall, 1987). Using relations between structure parameters and surface fluxes one can for instance derive the amount of evaporation from optical scintillation measurements. Probably because a convective boundary layer is dominated by one process, it is theoretically easier to describe than a stable boundary layer, and in the past more attention has been paid to it than to the stable boundary layer.

Due to the emission of longwave radiation of the land surface during the night the atmospheric boundary layer gets stably stratified. Vertical motion is restricted and turbulence is much weaker. Moreover the dynamics of the stable boundary layer may be influenced by more processes than continuous turbulence alone. Internal gravity waves (Finnigan and Einaudi, 1981), longwave radiation (André and Mahrt, 1982), and intermittent turbulence (Kondo et al., 1978) may be important and can complicate the structure of the stable boundary layer.

Observations of turbulence variables in general and of the structure parameter of temperature in particular in a stable boundary layer are not as abundant as in convective circumstances. Except for the data shown by Caughey et al. (1979), which are based on runs during the transition period, we are not aware of other observations of the structure parameter of temperature in the stable nocturnal boundary layer. In this paper we will use measurements, conducted at the meteorological mast at Cabauw, The Netherlands, to investigate the behaviour of the temperature structure parameter in a stable, nocturnal boundary layer. Only those nights which were characterized by continuous turbulence and which did not show the presence of significant gravity-wave activity were used.

We find that the structure parameter of temperature is large in the surface layer and decreases with increasing z/h, where h is the boundary layer height. The way the structure parameter decreases depends on the

particular shape of the temperature gradient, which in turn depends on the strength of the geostrophic wind and on time.

In section 2 we will discuss the experimental set-up and the procedure used to select the nights. The definition of the structure parameter of temperature will be discussed in section 3.
In section 4 models describing the vertical profile of the temperature structure parameter will be presented. The model of Nieuwstadt (1985) will be given in section 4a. In section 4b we derive the profile of the structure parameter using the similarity profiles for the stable continuous boundary layer published by Sorbjan (1986). Finally a short description of the model of Duynkerke and Driedonks (1987) is given in section 4c. In the last section we will show the observations and compare observations and models.

2. Observations

Between September 1977 and February 1979 and in August 1983 a series of nocturnal boundary layer experiments was carried out on the meteorological mast at Cabauw during clear nights when a stable, turbulent boundary layer was present (Nieuwstadt, 1984). The observations were started about 2-3 hours after sunset to avoid the transition period during which turbulence is dominated by non-stationary effects.

Table 1 The experimental set-up during nocturnal boundary layer experiments

Parameter	Instrument	Measuring height (m)
Turbulence	Trivane, fast thermocouple	20,40,80,120,160,200
Wind speed	Cup anemometer	10,20,40,80,120,160,200
Wind direction	Wind vane	20,40,80,120,160,200
Temperature	Ventilated thermocouples	10,20,40,80,120,160,200
Boundary layer height	Acoustic sounder	

The mast at Cabauw is 213 m high and the surrounding terrain is flat and homogeneous on a scale of approximately 20 km (Monna and van der Vliet, 1987). At height intervals of 20 m booms are installed in three directions. The instruments and measuring heights used during the experiments are given in Table 1.

Turbulent wind fluctuations were measured with a trivane (Wieringa, 1967 and 1972). A trivane consists of a propeller attached to one end of a rod, that can turn around two axes and is kept in the wind direction by means of an annular fin at the other end. The azimuth and elevation angle of the rod are determined by potentiometers.

Turbulent temperature fluctuations were measured from September 1977 to February 1979 with a pair of 100 µm copper-constantane thermocouples, mounted at both sides of the trivane (1 m apart). In August 1983 only one fast thermocouple was used. In Figure 1 examples of traces

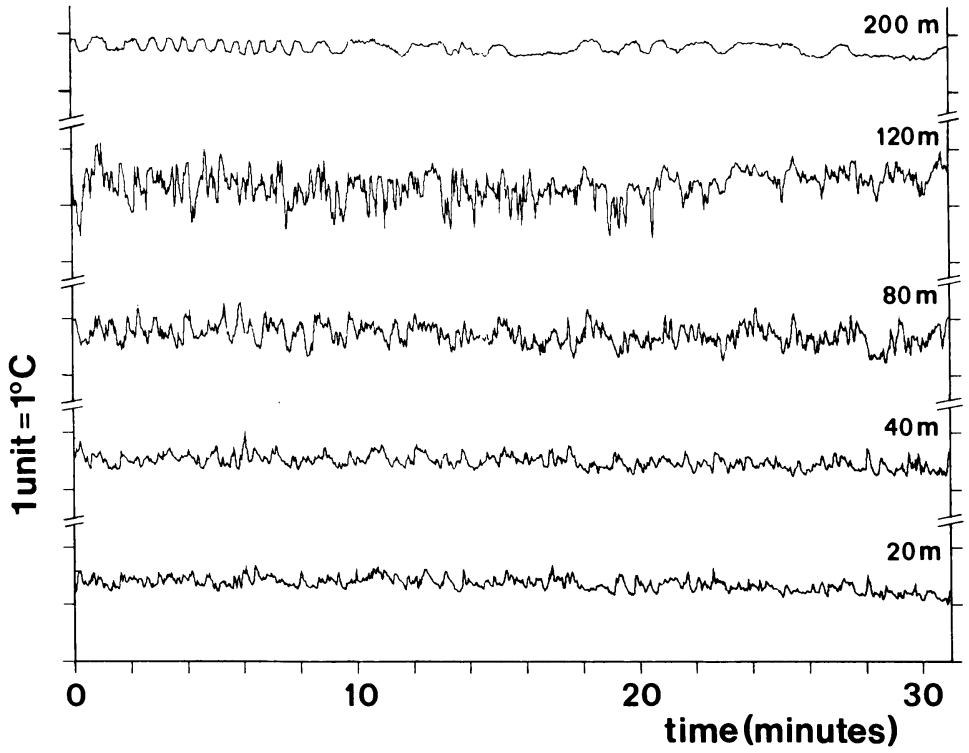

Fig.1 Temperature traces at several heights as a function of time, 20 Feb, 1978, 22:00 - 22:30 GMT. Temp. units in °C. (Geowind ≈ 11 m/s)

of the temperature as a function of time are shown for different heights. Observed vertical profiles of half-hourly mean potential temperature, wind speed and wind direction for the same period as Figure 1 are shown in Figure 2.

All turbulent data were sampled with a frequency of 5 Hz and stored on magnetic tape. Variances and covariances of the velocity and temperature fluctuations were calculated over a time period of 30 min. after removing a lineair trend from the time series. By this procedure only fluctuations with timescales $\lesssim$ 15 min. contribute to the (co)variances. The average wind speed, wind direction and temperature were determined over concurrent 30 min. periods.

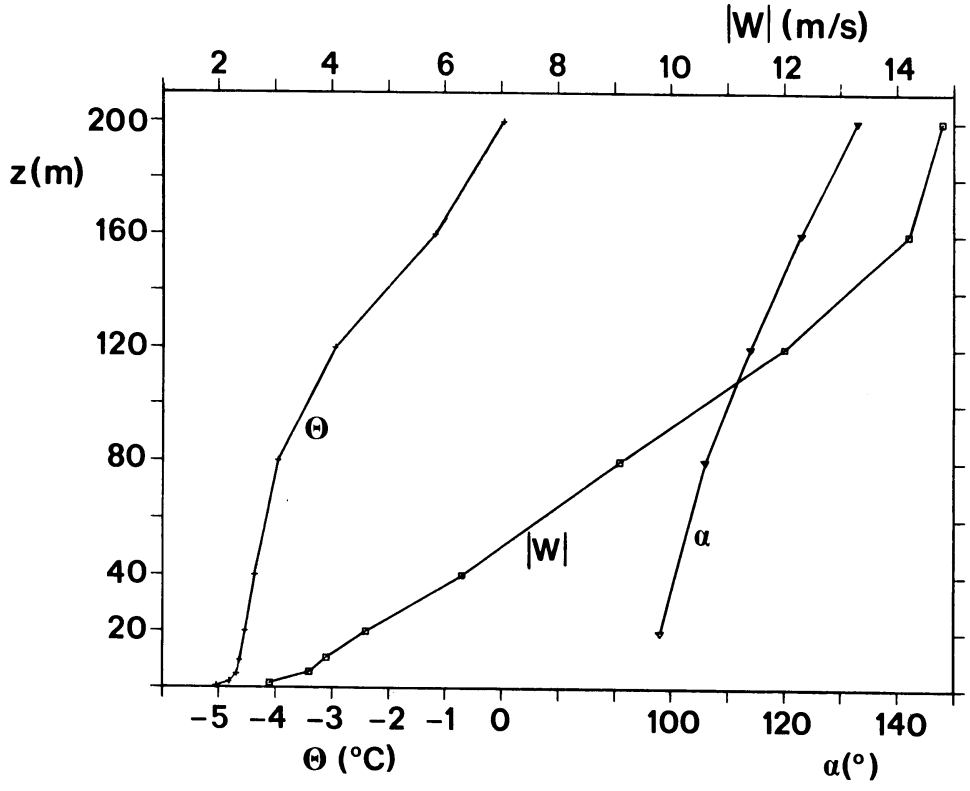

Fig.2 Measured vertical profiles of half-hourly mean potential temperature Θ, wind speed $|W|$ and wind direction α at Cabauw, 20 Feb, 1978, 22:00 - 22:30 GMT. The height of the boundary layer was 150 m.

Because only situations with continuous turbulence will be considered half-hour runs with a geostrophic wind speed ≥ 5 ms^{-1} were selected. In such cases the wind shear is large enough to maintain a continuous turbulent state. By using only those observations for which the vertical velocity variance decreases continuously with height we excluded boundary layers which are dominated by gravity waves (Driedonks and de Baas, 1983). Gravity waves are low-frequency buoyancy oscillations in a stably stratified atmosphere. Finally, we demanded that $h/L \geq 1$ (stability criterion), where h is the boundary layer height and L the Monin-Obukhov length. After this selection procedure 62 half-hour runs remained for the analysis of the structure parameter of temperature (Table 2).

Table 2

Half-hour runs used to determine structure parameter of temperature

Date	Observation period begin (GMT)	end (GMT)	Number of half hour runs
20/21 Feb 1978	19:00	06:00	17
19 May 1978	00:00	03:30	8
29/30 May 1978	23:00	01:00	4
31 May / 1 Jun 1978	22:30	02:00	8
26 Sep 1978	01:00	04:00	7
9 Feb 1979	04:30	08:00	7
30/31 Aug 1983	20:00	01:30	11

3. The structure parameter of temperature

In nature one often encounters fluctuating quantities like the fluctuating voltage appearing across a resistance in a state of thermodynamic equilibrium with the surrounding medium. Processes like these must be described by random functions. The value of such a function f(t) at a fixed instant of time is a random variable. However, in applications it is usually difficult to determine such functions.

Therefore in practice one uses statistical characteristics of the random function $f(t)$, the most important and simplest of which is the mean value $\overline{f(t)}$ (The overbar denotes averaging over the whole set of realizations of the function $f(t)$; in applications, this averaging is very often replaced by time averaging or space averaging).
Another important characteristic of the function is its correlation function $B_f(t_1, t_2)$ (Tatarski, 1961):

$$B_f(t_1, t_2) = \overline{[f(t_1) - \overline{f(t_1)}]\,[f(t_2) - \overline{f(t_2)}]} \; . \tag{3.1}$$

The correlation function $B_f(t_1, t_2)$ characterizes the mutual relation between the fluctuations of the quantity $f(t)$ at different instants of time. A random function $f(t)$ is called stationary if its mean value $\overline{f(t)}$ does not depend on time (here we shall assume that the mean value of a stationary function is zero) and if its correlation function $B_f(t_1, t_2)$ depends only on the difference $t_1 - t_2 = \tau$:

$$\overline{f(t)} = 0, \; B_f(t_1, t_2) = B_f(t_1 - t_2) = \overline{[f(t + \tau)\, f(t)]} \; . \tag{3.2}$$

In meteorology however, there also are quantities that show random fluctuations superimposed upon a gradual increase or decrease like for example temperature and wind speed. We now face the problem: which changes of the function $f(t)$ are random fluctuations and which are changes of the mean value? In order to describe these non-stationary random functions, in turbulence theory one uses so-called structure functions instead of correlation functions. For values of τ which are not too large, slow changes in the function $f(t)$ do not affect the value of $f(t + \tau) - f(t)$. This difference can be considered as a stationary random function of time; then, the function $f(t)$ is called a random function with stationary (first) increments.
The structure function $D_f(\tau)$ is defined by:

$$D_f(\tau) = \overline{[f(t + \tau) - f(t)]^2} \; . \tag{3.3}$$

Its value characterizes the intensity of those fluctuations of f(t) with periods smaller than or comparable to τ. When f(t) can be considered to be stationary within a certain period τ one can write:

$$D_f(\tau) = \overline{[f(t+\tau) - f(t)]^2} = \overline{[f(t+\tau)]^2} + \overline{[f(t)]^2} - \overline{2f(t+\tau)f(t)}, \qquad (3.4)$$

which equals:

$$D_f(\tau) = 2\,[B_f(0) - B_f(\tau)], \qquad (3.5)$$

because

$$\overline{[f(t)]^2} = \overline{[f\ (t + \tau)]^2} = \overline{B_f(0)}.$$

Fourier transform of the correlation function leads to the spectral function $W(\omega)$:

$$W(\omega) = \int_{-\infty}^{\infty} B_f(\tau)\, e^{-i\omega\tau}\, d\tau, \qquad (3.6)$$

where ω is the angular frequency.

Using (3.5) and (3.6) we find:

$$D_f(\tau) = 2 \int_{-\infty}^{\infty} [1-e^{i\omega\tau}]\, W(\omega)\, d\omega = 2 \int_{-\infty}^{\infty} [1 - \cos\,\omega\tau]\, W(\omega)\, d\omega. \qquad (3.7)$$

If the turbulent field does not change appreciably during the time of measurement τ, one can observe either the time behaviour of f(t) or f(r/U) at different points r in space, where U is the mean speed of the field. This approximation is referred to as the frozen-turbulence hypothesis. It is only valid if $\tau >> \frac{r}{U}$. By applying the frozen-turbulence hypothesis we obtain a relation between the structure function of a locally isotropic random field and the one-dimensional spectral density F(k):

$$D_f(r) = 2 \int_{-\infty}^{\infty} (1 - \cos\, kr)\, F(k)\, dk, \qquad (3.8)$$

where k is the spatial wavenumber.

The structure parameter of temperature is defined by:

$$C_T^2 = \frac{\overline{[T(x) - T(x + R)]^2}}{|R|^{2/3}} = D_T(R)\, R^{-2/3}, \qquad (3.9)$$

where $T(x)$ is the temperature at position x, and $T(x + R)$ that at $x + R$. The overbar indicates an ensemble average, which in practice is replaced by time averaging. C_T^2 is independent of R if the turbulence is homogeneous and isotropic and the separation $|R|$ is within the inertial subrange (Tatarski, 1961).

C_T^2 can be measured with two temperature sensors separated by a distance R, or with one sensor using measurements at different instants of time. In the latter case $T(x, t + \tau)$ is put equal to $T(x + R, t)$ with $R = U\,\tau$; U is the mean wind speed and τ is the time delay. Using equations (3.8) and (3.9) one can derived the spectrum for temperature fluctuations:

$$F_T(k) = 0.25\, C_T^2\, k^{-5/3}. \qquad (3.10)$$

An example of such a spectrum is shown in Figure 3. In this study we used eq. (3.10) to infer the temperature structure parameter C_T^2 from observed spectra. The error in the values of C_T^2 is estimated at 20%. Comparing (3.10) with Corrsin's inertial subrange form for temperature (Corrsin, 1951):

$$F_T(k) = 0.8\, N\, \varepsilon^{-1/3}\, k^{-5/3}, \qquad (3.11)$$

leads to:

$$C_T^2 = 3.2\, N\varepsilon^{-1/3}, \qquad (3.12)$$

where ε is the dissipation of turbulent kinetic energy and N is the dissipation of temperature variance. So, a fourth way to determine the structure parameter C_T^2 is by these molecular destruction terms. This method will be used in the models, described in the next section.

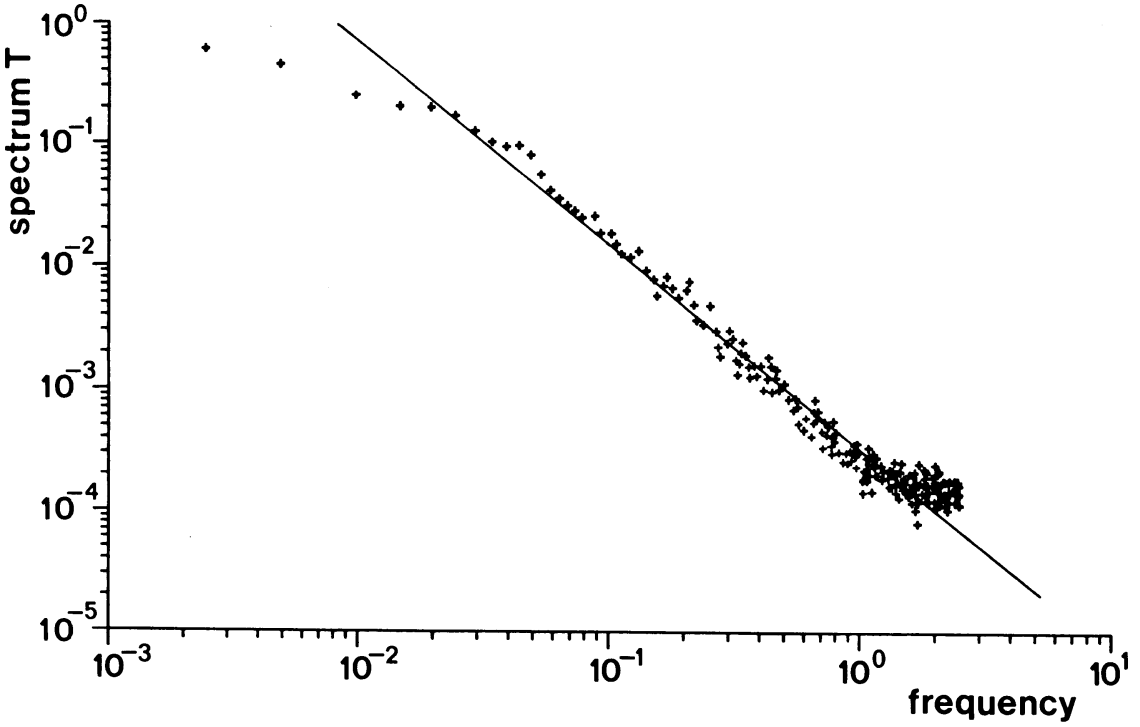

Fig.3 Temperature fluctuations spectrum, 20 Feb, 1978, 22:00 - 22:30 GMT. Measuring height was 40 m. The line indicates the -5/3 power.

4. The vertical profile of the temperature structure parameter: models

During night-time a stable boundary layer is mostly formed over a land surface. It is a shallow turbulent layer with a characteristic height of about 100 m. Several models have been developed to describe the nocturnal boundary layer. The model of Nieuwstadt (1984, 1985) is a description of turbulence to study the vertical structure of the stable boundary layer. In section 4a we will discuss this model and focus on the vertical profile of the structure parameter C_T^2. Another approach is offered by section 4b: once the vertical profiles of the Reynolds stress τ and the turbulent heat flux $\overline{w'\theta'}$ have been determined one can determine the vertical profile of C_T^2 using similarity theory. Duynkerke and Driedonks (1987) developed a multilevel ensemble-averaged model to study the cloud-topped atmospheric boundary layer. With this model the structure parameter C_T^2 can be calculated as a function of height. A discussion of this model will be given in section 4c.

4a. A model for the stationary, stable boundary layer

The evolution of the mean temperature Θ and the mean wind speed W in a horizontally homogeneous boundary layer can be described by:

$$\frac{\partial \Theta}{\partial t} = - \frac{\partial \overline{w'\theta'}}{\partial z} , \tag{4.1a}$$

$$\frac{\partial U}{\partial t} = f\,(V-V_g) - \frac{\partial \overline{u'w'}}{\partial z} , \tag{4.1b}$$

$$\frac{\partial V}{\partial t} = - f\,(U-U_g) - \frac{\partial \overline{v'w'}}{\partial z} , \tag{4.1c}$$

where U and V are the horizontal components of the wind speed W (the subscript g denotes geostrophic wind) and f is the Coriolis parameter. The turbulent heat flux is given by $\overline{w'\theta'}$. As a closure hypothesis for this set of equations it is assumed that the Richardson number, Ri, and the flux Richardson number, Ri_f, are constant:

$$Ri \equiv \frac{g}{T}\frac{\partial \Theta}{\partial z} \Big/ \left(\frac{\partial W}{\partial z}\right)^2 = \text{constant}, \tag{4.2a}$$

$$Ri_f \equiv - \frac{g}{T}\overline{w'\theta'} \Big/ \tau \frac{\partial W}{\partial z} = \text{constant}, \tag{4.2b}$$

where τ is given by: $\tau=[\overline{(-u'w')}^2 + \overline{(-v'w')}^2]^{1/2}$. Only a stationary, stable boundary layer will be considered, thus the fluxes are independent of time. This restriction has the following consequences. From (4.1a) one finds that the cooling rate $\frac{\partial \Theta}{\partial t}$ is a constant, from (4.2b) that the (vertical) velocity gradient must be independent of time and with equation (4.2a) it follows that the temperature gradient is also independent of time. By considering the gradients of these equations the time derivatives will then disappear. We get, assuming $\partial U_g/\partial z = \partial V_g/\partial z = 0$:

$$0 = \frac{\partial^2 \overline{w'\theta'}}{\partial z^2} , \tag{4.3a}$$

$$0 = f \frac{\partial V}{\partial z} - \frac{\partial^2 \overline{u'w'}}{\partial z^2} , \tag{4.3b}$$

$$0 = - f \frac{\partial U}{\partial z} - \frac{\partial^2 \overline{v'w'}}{\partial z^2} . \tag{4.3c}$$

In order to solve this set of equations it is convenient to use the following non-dimensional parameters:

$$\sigma = \tau/u_*^2 \ , \tag{4.4a}$$

$$H = \overline{w'\theta'} \ / \ \overline{w'\theta'_o} \ , \tag{4.4b}$$

$$\eta = z/h \ , \tag{4.4c}$$

$$S = \frac{L}{u_*} \frac{\partial W}{\partial z} \ , \text{ and} \tag{4.4d}$$

$$\gamma = \frac{L}{T_*} \frac{\partial \Theta}{\partial z} \ . \tag{4.4e}$$

The friction velocity u_*, the surface heat flux $\overline{w'\theta'_o}$, the temperature scale T_* and the Obukhov-length L are defined by:

$$u_*^2 = ||\tau(0)|| \ , \ \overline{w'\theta'_o} = \overline{w'\theta'}\ (0), \tag{4.5a}$$

i.e. the surface values of stress and heat flux,

$$T_* = - \overline{w'\theta'_o} \ / \ u_* \ , \tag{4.5b}$$

$$L = - u_*^3 \ / \ (k \ g/T \ \overline{w'\theta'_o}) \ , \tag{4.5c}$$

where k is the von Karman constant.

With these variables (4.3a-c) and (4.2a-b) become

$$\frac{\partial^2 H}{\partial \eta^2} = 0 \ , \tag{4.6a}$$

$$\frac{\partial^2 \sigma}{\partial \eta^2} - i \ c^2 \ S = 0 \ , \tag{4.6b}$$

$$\frac{\gamma}{||S||^2} = k \ Ri \ , \tag{4.6c}$$

$$\frac{H}{\sigma * S} = k \ Ri_f \ , \tag{4.6d}$$

where the parameter c is defined by:

$$c = h \,/\, \left(\frac{u_* L}{f}\right)^{1/2}. \tag{4.7}$$

A complex notation is used here, so that $W = U + iV$ and $\tau = \tau_x + i\,\tau_y$ (σ^* is the complex conjugate of σ). The boundary conditions for this set of equations are given by:

$$\sigma = 1,\ H = 1 \text{ for } \eta = 0, \tag{4.8a}$$

$$\sigma = 0,\ H = 0 \text{ for } \eta = 1, \tag{4.8b}$$

which means that the turbulent fluxes equal their surface values at $\eta = 0$ and that turbulence vanishes at the top of the boundary layer.

By integrating (4.6a) we find a lineair profile for the heat flux:

$$\overline{w'\theta'} \,/\, \overline{w'\theta'_o} = 1 - z/h. \tag{4.9}$$

Using this equation we can eliminate S from (4.6b) and (4.6d):

$$\sigma^* \frac{\partial^2 \sigma}{\partial \eta^2} - ic^2 \frac{1}{k\, Ri_f} (1-\eta) = 0\ . \tag{4.10}$$

With the boundary conditions (4.8a-b) and $c^2 = \sqrt{3}\ k\, Ri_f$ a solution of this equation is:

$$\sigma = (1-\eta)^{1/2} (3 + i\sqrt{3})\ , \tag{4.11a}$$

or:

$$||\tau|| \,/\, u_*^2 = (1-z/h)^{3/2}. \tag{4.11b}$$

Using these solutions for the profiles of the turbulent stress and heat flux (which according to several observations seems to be reasonable for the stable boundary layer) and (4.6c-d) leads to the production terms of turbulent kinetic energy and temperature variance:

$$\tau \frac{\partial W}{\partial z} = \frac{1}{k\, Ri_f} \frac{u_*^3}{L} (1 - z/h) , \qquad (4.12a)$$

$$- \overline{w'\theta'} \frac{\partial \theta}{\partial z} = - \frac{Ri}{k\, Ri_f} \frac{T_*}{L} \overline{w'\theta'_o} . \qquad (4.12b)$$

The molecular destruction terms ε and N can be found from the turbulent kinetic energy and temperature variance budgets:

$$\frac{\partial E}{\partial t} = \tau \frac{\partial W}{\partial z} + \frac{g}{T} \overline{w'\theta'} - \frac{\partial}{\partial z} (\overline{w'E'} + \overline{p'w'}/\rho) - \varepsilon, \qquad (4.13a)$$

$$\frac{1}{2} \frac{\partial \overline{\theta'^2}}{\partial t} = - \overline{w'\theta'} \frac{\partial \theta}{\partial z} - \frac{\partial}{\partial z} \left(\frac{1}{2} \overline{w'\theta'^2}\right) - N , \qquad (4.13b)$$

where p' are pressure fluctuations (Businger, 1982). The time variation can be neglected because a stationary boundary layer is assumed. Brost and Wyngaard (1978) showed that vertical transport is small in a stable boundary layer, so that the terms $\frac{\partial}{\partial z} (\overline{w'E'} + \overline{p'w'}/\rho)$ and $\frac{\partial}{\partial z} \left(\frac{1}{2} \overline{w'\theta'^2}\right)$ can be neglected. From (4.12a) - (4.13b) we then find the following dimensionless equations, that describe the vertical profiles of the destruction terms ε and N:

$$\frac{kh\varepsilon}{u_*^3} = \frac{1-Ri_f}{Ri_f} \frac{h}{L} (1 - z/h) , \qquad (4.14a)$$

$$\frac{khN}{T_*^2\, u_*} = \frac{Ri}{Ri_f^2} \frac{h}{L} . \qquad (4.14b)$$

Note that the temperature dissipation N is independent of height. We can see this also in the following way: by substitution of (4.9) and (4.11a) into (4.6c) and (4.6d) we obtain:

$$\gamma = \frac{Ri}{k\, Ri_f^2} (1-\eta)^{-1} . \qquad (4.15)$$

We note that $\frac{\partial \theta}{\partial z}$ is proportional to $(1-z/h)^{-1}$. Because $\overline{w'\theta'}$ is proportional to (1-z/h) we obtain $N = -\overline{w'\theta'} \frac{\partial \theta}{\partial z}$ is independent of height.

Now we can use relation (3.12), $C_T^2 = 3.2\, N\, \varepsilon^{-1/3}$, to find the vertical profile of the structure parameter of temperature:

$$\frac{C_T^2 (kh)^{2/3}}{T_*^2} = 3.2 \frac{Ri}{Ri_f^{5/3} (1-Ri_f)^{1/3}} \left(\frac{h}{L}\right)^{2/3} (1-z/h)^{-1/3} \quad . \quad (4.16)$$

Towards the surface C_T^2 approaches to a constant value. This value and consequently the whole profile is a function of the stability parameter h/L. The value for Ri and Ri_f that has been used to find (4.9) and (4.11), is taken to be 0.2, which seems to be a reasonable assumption for a major part of the boundary layer (Figure 4).
C_T^2 increases with height. The profile of C_T^2 is determined by the profile of ε solely, because, as noted above, N is constant with height. Figure 5 shows the calculated profiles of the dimensionless structure parameter $CTN = \frac{C_T^2 (kh)^{2/3}}{T_*^2}$ for different values of the stability parameter h/L. Note that for z/h -> 1, CTN becomes infinite.

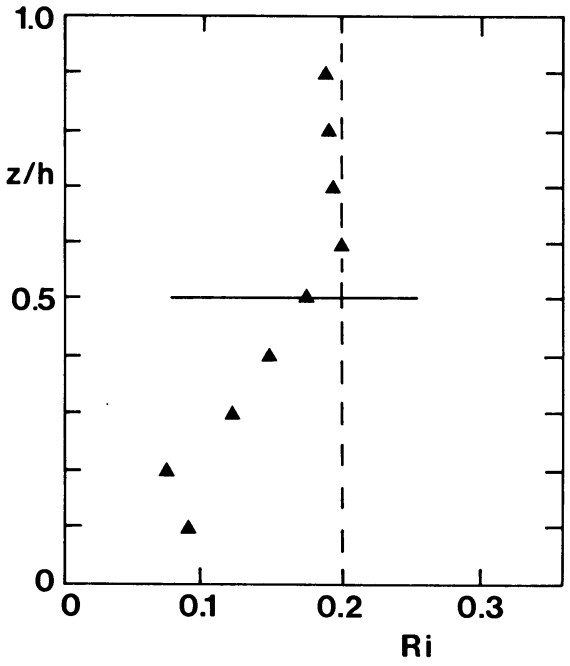

Fig.4 The Richardson number as a function of non-dimensional height. Each point indicates the average of all observations within a given height interval. The horizontal bar indicates the standard deviation of the data (from Nieuwstadt, 1985).

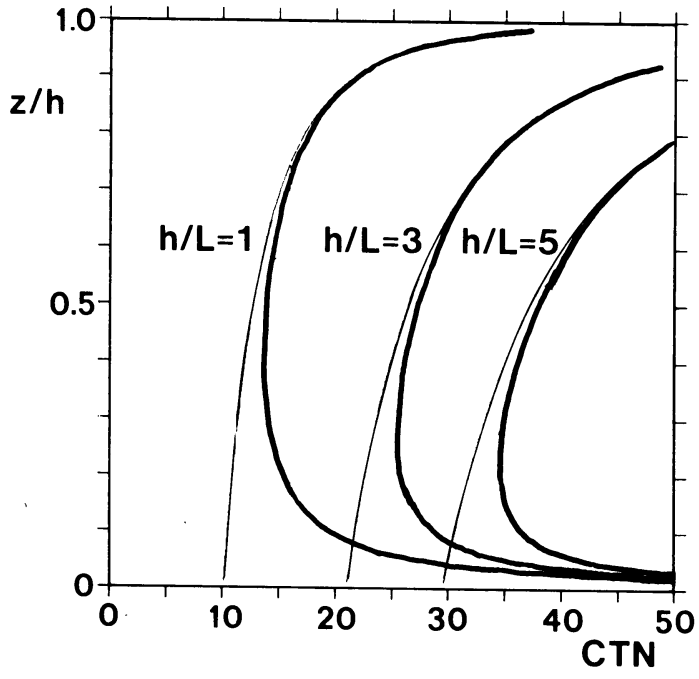

Fig.5 Calculated profiles of the dimensionless structure parameter for different values of the stability parameter h/L. The thin lines are according to Nieuwstadt's model. The thick lines according to (4.24) with the constants α_1 and α_2 of Nieuwstadt, i.e. $\alpha_1 = 1.5$ and $\alpha_2 = 1$.

4b. The profile of C_T^2 using similarity functions

In 1954, Monin and Obukhov published a paper on the similarity theory of the surface layer. According to this theory the non-dimensional wind shear and temperature gradients must be functions of $\zeta = z/L$ only:

$$\frac{kz}{u_*}\frac{\partial W}{\partial z} = \phi_m(\zeta), \tag{4.17a}$$

$$\frac{kz}{T_*}\frac{\partial \theta}{\partial z} = \phi_h(\zeta). \tag{4.17b}$$

The theory is a great help in the analysis of the mean flow in the atmospheric boundary layer. However, similarity theory does not help to determine the shapes of the functions ϕ_m and ϕ_h. They can only be determined by experiments. Yaglom (1977) gives an authoritative review of the many different formulas for ϕ_m and ϕ_h that have been proposed in the literature. A generally used version of the functions ϕ_m and ϕ_h is (Dyer, 1974):

$$\phi_m = \phi_h = 1 + 5\,\zeta. \tag{4.18}$$

Nieuwstadt (1984) introduced the idea of local scaling for the stable boundary layer. Dimensionless combinations of variables which are measured at the same height (therefore the term local is used) can be expressed as a function of a single parameter z/Λ solely, where Λ is the local Obukhov-length:

$$\Lambda = -\tau^{3/2} / (k\, g/T\, \overline{w'\theta'}) \,. \tag{4.19a}$$

The local values of the Reynolds stress $\tau(z)$ and the turbulent heat flux $\overline{w'\theta'}(z)$ define the local friction velocity $U_*(z)$ and temperature scale $t_*(z)$:

$$U_*(z) = \tau^{1/2}, \tag{4.19b}$$

$$t_*(z) = -\overline{w'\theta'} / \tau^{1/2}. \tag{4.19c}$$

Nieuwstadt showed that the observations taken at Cabauw support local scaling.

Using these local variables one can define the following similarity functions:

$$\Phi_m = \frac{kz}{U_*}\frac{\partial W}{\partial z}\,, \tag{4.20a}$$

$$\Phi_h = \frac{kz}{t_*}\frac{\partial \theta}{\partial z}\,, \tag{4.20b}$$

$$\Phi_\varepsilon = \Phi_m - Z = \frac{kz\varepsilon}{U_*^3}\,, \tag{4.20c}$$

where $Z = z/\Lambda$. These functions must approach to the Monin-Obukhov functions for $z \to 0$. Therefore, Sorbjan (1986) introduced the next hypothesis:
"The form of the similarity functions Φ of Z in the outer layer (the part of the boundary layer above the surface layer) is identical to the form of Monin-Obukhov similarity functions ϕ of ζ in the surface layer". This leads to:

$$\Phi_m = \Phi_h = 1 + 5\,Z, \tag{4.21a}$$

$$\Phi_\varepsilon = 1 + 4\,Z. \tag{4.21b}$$

Next, Sorbjan assumed that the vertical profiles of stress and heat flux are given by:

$$\tau = u_*^2\,(1-z/h)^{\alpha_1}, \tag{4.22a}$$

$$\overline{w'\theta'} = \overline{w'\theta'_o}\,(1-z/h)^{\alpha_2}. \tag{4.22b}$$

The constants α_1 and α_2 depend among others on the state of the stable boundary layer and terrain slope and must be determined emperically. Observations give values between 1 and 2 for α_1 and values between 1 and 3 for α_2 (Lacser and Arya, 1986). One further expects that the gradients of temperature and wind speed will remain finite throughout the boundary layer. With (4.20), (4.21) and (4.22) this leads to the following restriction for the vertical profiles: $\alpha_2 \geq \alpha_1$. Because of large scatter

in the data the constants α_1 and α_2 are rather difficult to obtain for one single night. Using all his observations Nieuwstadt (1984) found $\alpha_1 = 1.5$ and $\alpha_2 = 1$, so the restriction $\alpha_2 \geq \alpha_1$ was not confirmed by his data set. The fact that these values are overall means might have caused this result.

Using (4.19) and (4.22) we find the next relations between local quantities and surface quantities:

$$U_* = u_* \, (1 - z/h)^{\alpha_1/2}, \tag{4.23a}$$

$$t_* = T_* \, (1 - z/h)^{\alpha_2 - \alpha_1/2}, \tag{4.23b}$$

$$\Lambda = L \, (1 - z/h)^{3/2\alpha_1 - \alpha_2}. \tag{4.23c}$$

With these relations and (4.20), (4.21) and (3.12) we obtain the vertical profile for the structure parameter of temperature in dimensionless form:

$$\frac{C_T^2 (kh)^{2/3}}{T_*^2} = 3.2 \, \frac{(5 \, \mu \, z/h + (1-z/h)^{3/2 \, \alpha_1 - \alpha_2})}{(4 \, \mu \, z/h + (1-z/h)^{3/2 \, \alpha_1 - \alpha_2})^{1/3}} \, \frac{(1-z/h)^{8/3 \, \alpha_2 - 2\alpha_1}}{(z/h)^{2/3}}, \tag{4.24}$$

where $\mu = h/L$ is the stability parameter.

In Figure 5 we show the profiles of the dimensionless structure parameter CTN for different values of the stability parameter h/L and the constants α_1 and α_2 of Nieuwstadt. For $z/h \geq 0.35$ (4.24) gives the same results as Nieuwstadt's model, which is only valid for $z/L >> 1$. Using this restraint and the constants of Nieuwstadt in (4.24) we obtain:

$$\frac{C_T^2 (kh)^{2/3}}{T_*^2} \approx 3.2 \, C \, (h/L)^{2/3} \, (1 - z/h)^{-1/3}, \tag{4.25}$$

where the constant $C = 5 \, / \, 4^{1/3} = 3.15$ equals the factor

$\frac{Ri}{Ri_f^{5/3}(1-Ri_f)^{1/3}}$ in (4.16) with $Ri = Ri_f = 0.2$. It now becomes clear that the closure hypothesis $Ri = Ri_f$ = constant causes the structure parameter to become constant near the surface. However, observations show that near the surface the values of Ri and Ri_f deviate from 0.2 (Fig. 4). When similarity functions are used the influence of the surface layer is taken into account. So, we expect that the shape of the structure parameter profile in that part of the boundary layer will be better described by (4.24) than by Nieuwstadt's model.

We note further that CTN always increases near the surface irrespective of $\alpha_2 > \alpha_1$ or $\alpha_2 < \alpha_1$. However, for larger z/h the shape of the profile does depend on the value of α_2/α_1. For $\alpha_2 > \frac{3}{4}\alpha_1$, CTN -> 0 at the top of the boundary layer, whereas for $\alpha_2 < \frac{3}{4}\alpha_1$ the structure parameter of temperature goes to infinity. With the earlier restriction of $\alpha_2 \geq \alpha_1$, it follows that (4.24) describes a decreasing structure parameter with height (Figure 6), whereas, adopting Nieuwstadt's values $\alpha_1 = 1.5$ and $\alpha_2 = 1$, CTN -> ∞ at the top of the boundary layer (Fig. 5).

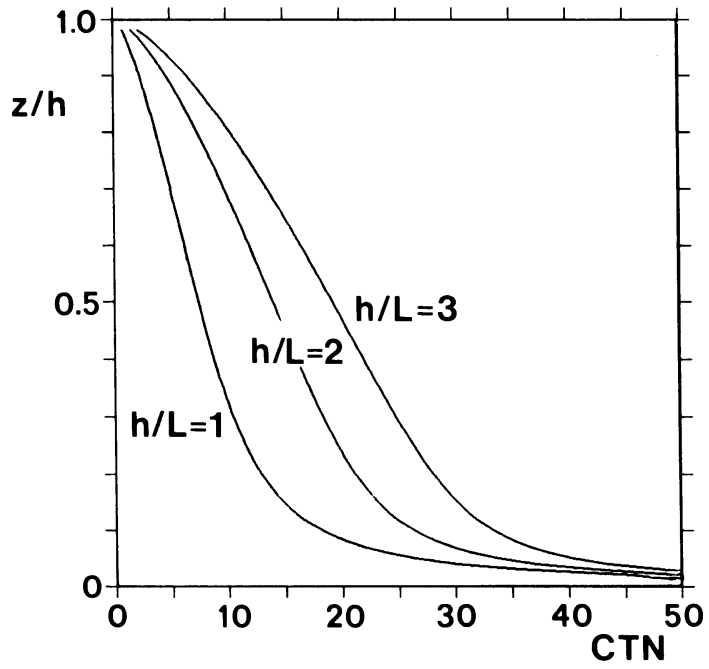

Fig.6 The profiles of the dimensionless structure parameter using (4.24) with $\alpha_1 = \alpha_2 = 1$.

4c. C_T^2 calculated with a multilevel ensemble-averaged model

To study the cloud-topped atmospheric boundary layer Duynkerke and Driedonks (1987) developed a multilevel ensemble-averaged model. In this type of model the combined effect of all eddy sizes has to be parameterized. For this purpose several turbulent closure hypotheses have been developed. They are mainly based on observational data from the clear-sky atmospheric boundary layer. In the model of Duynkerke and Driedonks turbulence closure is formulated by using an equation for the turbulent kinetic energy and a diagnostic formulation for the length scale.

The ensemble-averaged equations describing the dynamics of the atmospheric boundary layer in horizontally homogeneous conditions are a more complete version of (4.1). Duynkerke et al. added to these equations an equation that describes the evolution of total water, i.e. water vapor and liquid water. We adopted a low humidity in order to prevent cloud formation. Moreover, the humidity is taken independent of time and no evaporation has been taken into account.

The fluxes in the equations are expressed as:

$$-\overline{\phi' w'} = K_{m,h} \frac{\partial \phi}{\partial z} , \tag{4.26}$$

where ϕ is either a horizontal velocity component (K_m is used), or temperature or specific humidity (K_h). The exchange coefficients are calculated with:

$$K_{m,h} = c\, l_{m,h}\, E^{1/2} , \tag{4.27}$$

where c is a constant, $l_{m,h}$ a length scale and E the turbulent kinetic energy, determined by a more complete version of (4.13a). In the stable boundary layer the length scale $l_{m,h}$ is determined by a suitable interpolation between two length scales; viz. a length scale for the surface layer:

$$l = kz/\phi_{m,h}, \tag{4.28a}$$

with $\phi_{m,h} = 1 + 5\ z/L$, and a length scale for the stable layer:

$$l_s = c_s\ E^{1/2}\ /N, \qquad (4.28b)$$

where $c_s = 0.36$ and N is the Brunt-Väisälä frequency given by:

$$N^2 = \frac{g}{\theta_o}\frac{\partial\theta}{\partial z}\ . \qquad (4.28c)$$

The longwave radiative cooling of the atmosphere is calculated with the bandmodel of Tjemkes (priv. comm.), the surface temperature with a model of Deardorf (1978). For the roughness length a value of 0.15 m is adopted, which is typical for the Cabauw surroundings. The calculations were started with a neutral temperature profile.

Two situations, one with a geostrophic wind of 6 m/s and the other with 10 m/s have been simulated. In Figure 7 the curves are shown after 4h, 6h, 8h and 10h.

With a geostrophic wind of 6 m/s there is a continuous decrease of the structure parameter with height. The stability parameter h/L for this case is about 3. With a geostrophic wind of 10 m/s only in the beginning of the night a continuous decrease of the structure parameter is seen. After about 6h the structure parameter decreases with height only in the lower half of the boundary layer, while in the upper half it reaches a maximum at $z/h \approx 0.7$, after which it decreases again down to a small value at the top of the boundary layer. During the night the whole curve above $z/h \approx 0.1$ moves to the right. This means an increase of the structure parameter in the entire boundary layer, which is most pronounced around $z/h \approx 0.6 - 0.7$. However, there is also a slight decrease of the stability parameter h/L from $h/L \approx 2.5$ to $h/L \approx 2.0$. We thus observe that CTN increases with decreasing h/L. In contrast Nieuwstadt's model predicts an increase of the structure parameter with increasing h/L (Eq. (4.16)). Moreover, the profiles of Nieuwstadt's model disagree with the model of Duynkerke et al. On the other hand, there is a reasonable agreement between the profiles of the model of Duynkerke et al. with a geostrophic wind speed of 6 m/s and the profile following from Sorbjan's hypothesis, Eq. (4.24), with $\alpha_1 = \alpha_2 = 1$. However, the profiles with $W_{geo} = 10$ m/s do not agree with (4.24) for any value of α_1 and α_2.

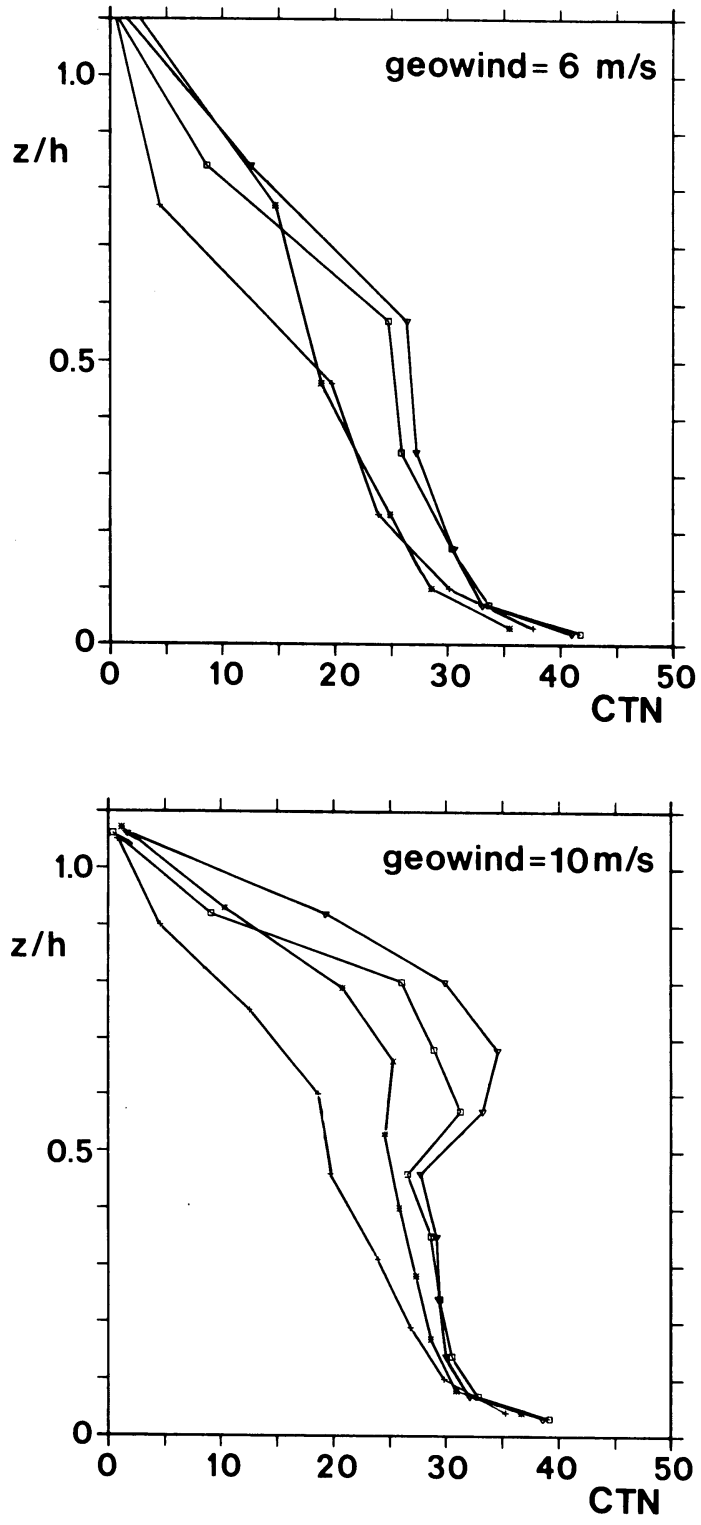

Fig.7 Profiles of the dimensionless structure parameter calculated with the model of Duynkerke and Driedonks. Curves are shown after 4h (+), 6h (*), 8h (□) and 10h (▽).

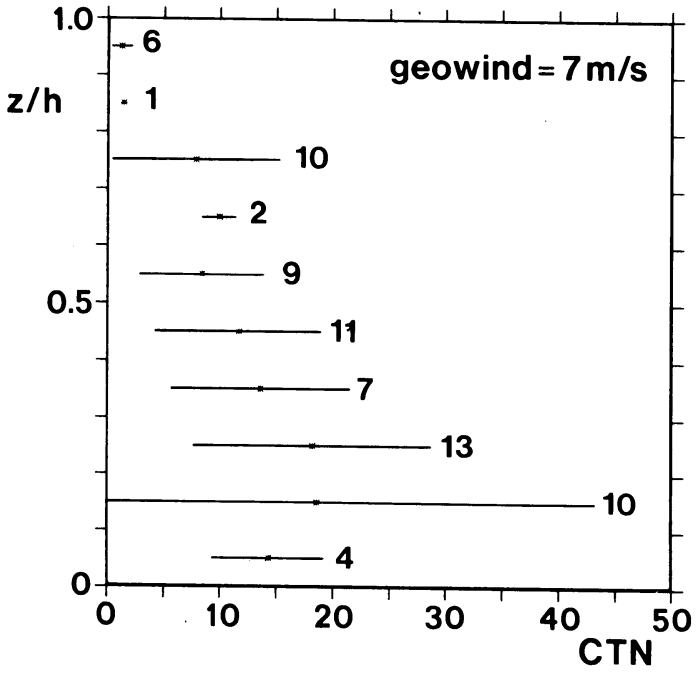

Fig.8 Observations of the dimensionless structure parameter for low geostrophic wind periods and high geostrophic wind periods at the beginning of the night. The wind speed is the mean of the low geostrophic wind periods only. Each point indicates the average of all observations within a given height interval. The bar indicates the standard deviation of the data and the number represents the number of data points within each height interval.

5. Results and discussion

In Figures 8 and 9 we show observations of the dimensionless structure parameter CTN for the periods mentioned in Table 2. The mean geostrophic wind speed during the observation periods is indicated. From these figures it appears that the structure parameter is large near the surface and small at the top of the boundary layer. The profiles between surface layer and inversion layer can roughly be devided into two classes. First, there are observation periods when CTN decreases continuously with height. In these periods the geostrophic wind speed is about 7 m/s or there is a higher geostrophic wind speed but observations where done early at night (Fig. 8). Second, in the other periods (with $W_{geo} \approx 11$ m/s and observations done later at night) CTN decreases in the lower half of the boundary layer, but shows an increase about $z/h \approx 0.7$, after which it decreases again (Fig.9).

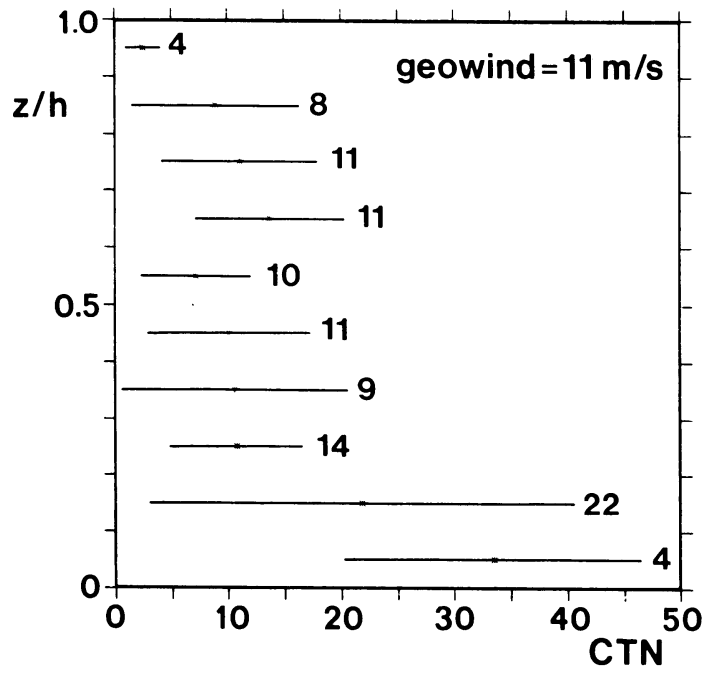

Fig.9 As Fig. 8, but now for high geostrophic wind periods later at night. The mean geostrophic wind speed in these periods is indicated.

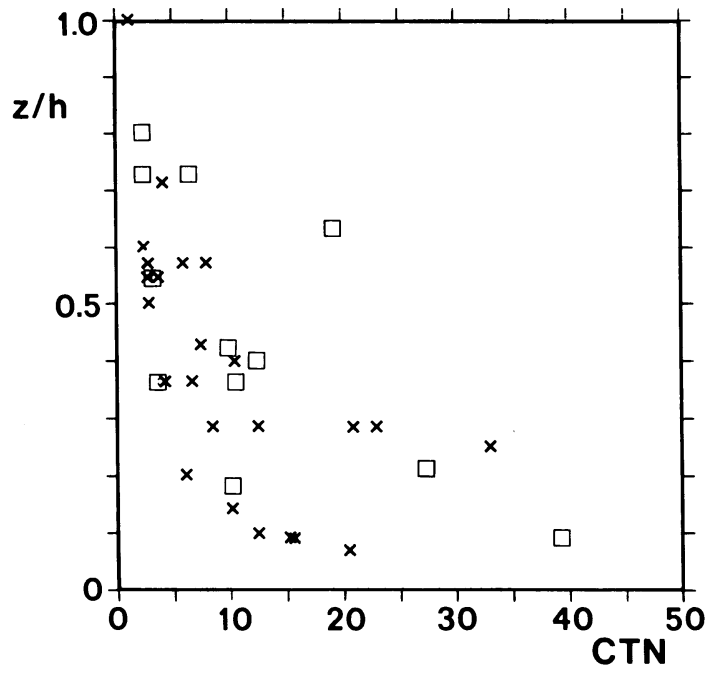

Fig.10 Observations of the dimensionless structure parameter with the stability parameter either in the interval $1.0 \leq h/L < 1.5$ (x) or $5.5 \leq h/L < 7.0$ (□).

In Figure 10 we show observations of CTN as a function of z/h where only those values of CTN were used with the stability parameter either in the interval $1.0 \leq h/L < 1.5$ or $5.5 \leq h/L < 7.0$. According to Nieuwstadt's expression (4.16) CTN should be about three times as large in the latter case as in the first case (Fig.5). However, the observations do not show such a behaviour. The observed structure parameter does not seem to depend on the stability parameter.

In section 4a we concluded that according to Nieuwstadt's theory the temperature structure parameter approaches to a constant value at the surface and increases with height. The observations on the contrary show that the structure parameter increases near the surface and is small at the top of the boundary layer. The reason for the discrepancy in the surface layer is that Ri and Ri_f were assumed to be constant (0.2). Near the surface Ri and Ri_f are smaller than 0.2 due to the high shear production. At the top of the boundary layer the assumption seems

correct. The second assumption in Nieuwstadt's theory, that of stationarity is likely to cause the theoretical profile to become infinite, which behaviour is not supported by the observations. As a consequence of this assumption $\frac{\partial\theta}{\partial z}$ is proportional to $(1-z/h)^{-1}$. Then the dissipation of temperature variance N is independent of height and consequently, the profile of CTN is determined by the profile of the dissipation of turbulent kinetic energy ε only (section 4a). However, if $\frac{\partial\theta}{\partial z}$ is proportional to $(1-z/h)^{-1}$ then θ increases continuously with height to become infinite at the top of the boundary layer. Fig. 11 shows that this is not the case. So, $\frac{\partial\theta}{\partial z}$ is not proportional to $(1-z/h)^{-1}$. Therefore, N must be a function of height and the profile of CTN is determined by the profiles of ε and N.

Next, we turn to the model of Sorbjan. We first examine the dimensionless profiles of the temperature and wind gradient (4.20). Observations of these so-called similarity functions Φ_m and Φ_h are shown in Figures 12a and 12b. In the same figures lines $1 + \beta\ z/\Lambda$ with $\beta = 5$ and $\beta = 10$ are drawn. For small values of z/Λ the lines with $\beta = 10$ seems to fit better, whereas for larger z/Λ $\beta = 5$ seems to be more appropriate.

The profile of the structure parameter in the surface layer is in an acceptable way described by using similarity functions of Sorbjan. However, above this layer the profile is sensitive to the specific values of α_1 and α_2 of the stress and heat flux profiles (eq. (4.22)). For a single night these values could not be determined because of large scatter in the data. But whatever choices of α_1 and α_2 are made, the profile of CTN above the surface layer will be either continuously increasing or decreasing. So, even if one were able to determine these constants one could only expect good agreement in moderate geostrophic wind speed cases. The model can not generate the maximum of CTN observed in the upper mixed layer for the high wind speed cases. Moreover, like the model of Nieuwstadt (section 4a), also here the profile of CTN is a function of h/L. The more stable the atmosphere, the larger CTN is. As we saw before the observations do not show such a behaviour (Fig.10).

The best agreement with observations is found with the profiles calculated by the model of Duynkerke and Driedonks (1987). The calculated profiles show an increase near the surface. For medium geostrophic winds (~ 6 m/s) we have a continuous decrease of CTN towards the top of

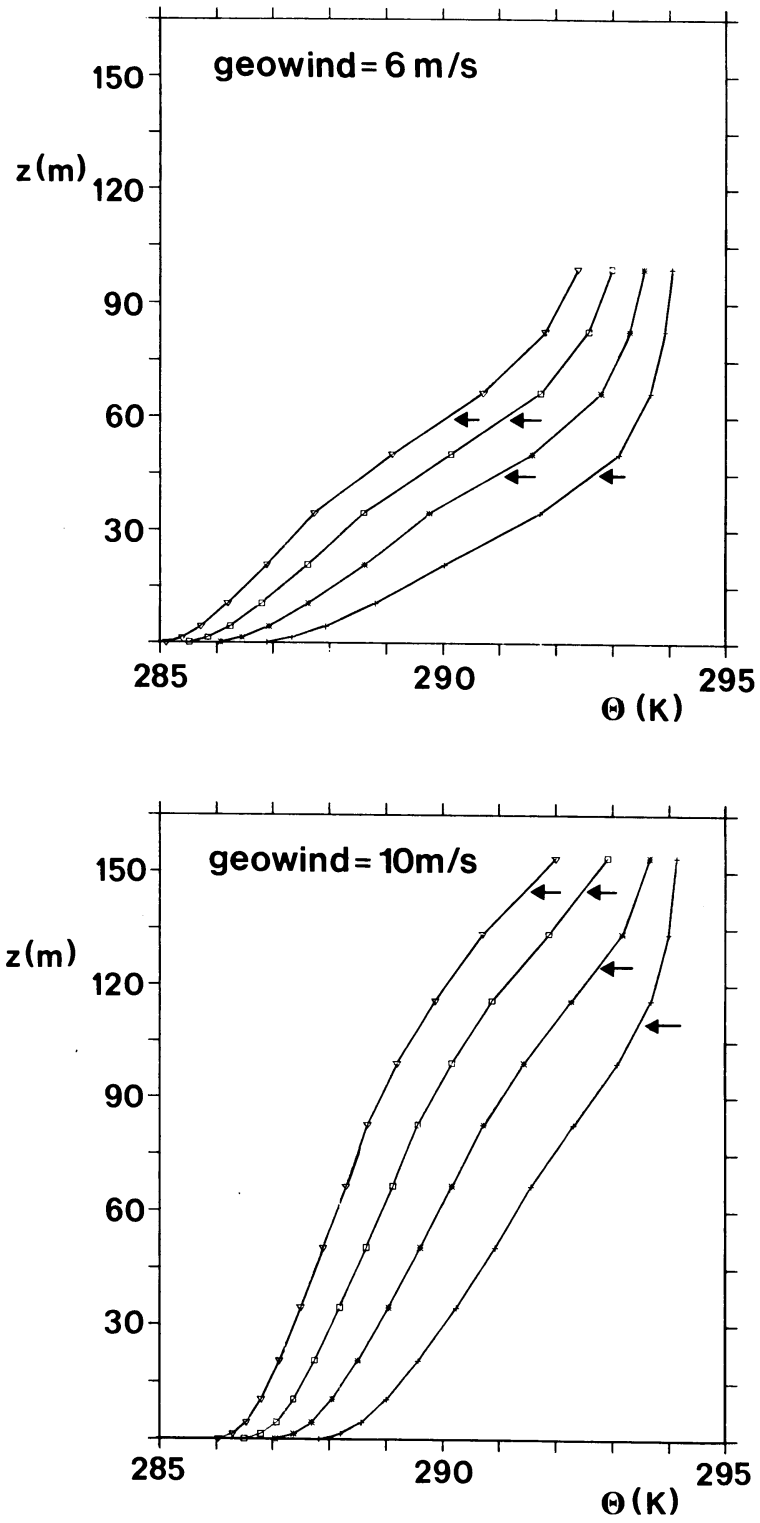

Fig.11 Potential temperature profiles computed for two values of the geostrophic wind after 4h (+), 6h (*), 8h (□) and 10h (▽). The boundary layer height, defined as the altitude where the heat flux is 5% of its surface value, is indicated by an arrow.

the boundary layer. In the situation of a strong geostrophic wind the model shows that, after a few hours, a maximum of CTN develops about $z/h \approx 0.7$. So, the shapes of the calculated profiles agree qualitatively with observed profiles. However, the values of CTN found with the model are about 2-3 times as high as those observed. The reason for this is not clear to us. It might be (partially) caused by the similarity functions used in the model. As pointed out above the shape of these functions for small values of z/Λ is $1 + 10\ z/\Lambda$ rather than $1 + 5\ z/\Lambda$. The model uses a similarity function $1 + 5\ z/L$ in the surface layer, where $L \approx \Lambda$. An increase of $\phi_{m,h}$ will decrease the exchange coefficients $K_{m,h}$ and consequently the vertical exchange will be less. Then CTN is expected to be less, too.

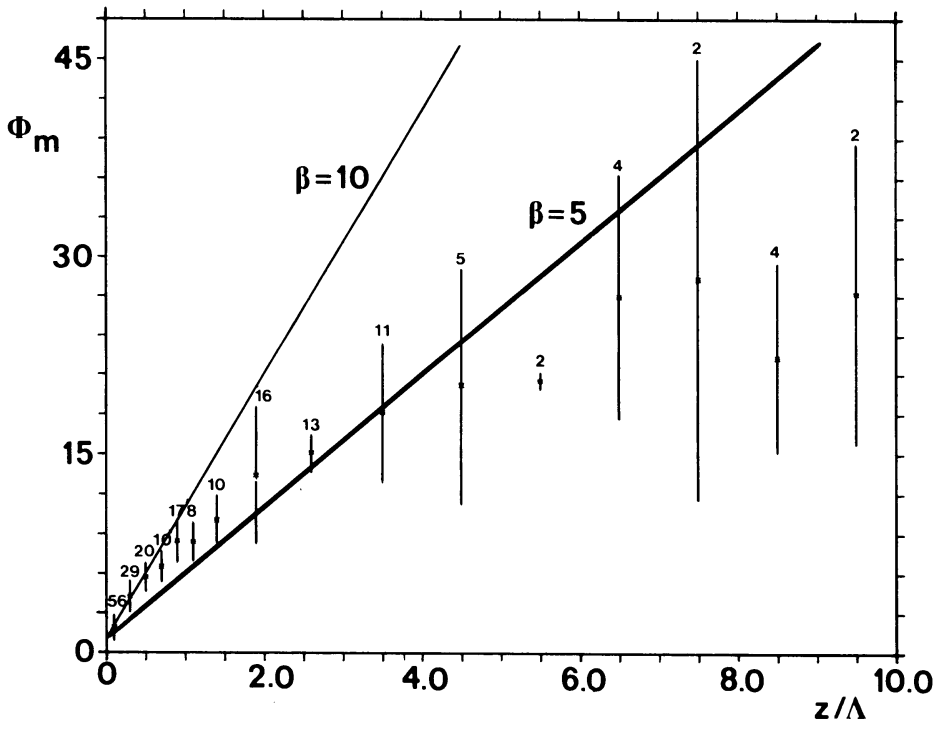

Fig.12a Dimensionless profile of wind gradient Φ_m as a function of the dimensionless height z/Λ. Symbols as in Fig.8. Also shown is the function $\Phi = 1 + \beta\ z/\Lambda$ with $\beta = 5$ (thick line) and $\beta = 10$ (thin line).

The behaviour of the structure parameter of temperature can roughly be understood using the profiles of potential temperature (Fig.11). In the low geostrophic wind case there is a large temperature gradient close to the surface. In that region there is much mechanical turbulence and CTN is large. Higher in the boundary layer vertical exchange and consequently turbulence is suppressed because of stable stratification. The vertical temperature gradient decreases continuously with height and so does CTN which depends on it (see eq. (3.12) and (4.13b)). For strong wind conditions the situation is similar at the beginning of the night. However, after a few hours we see an increase of the temperature gradient at larger height. This causes the increase of CTN at $z/h \approx 0.7$.

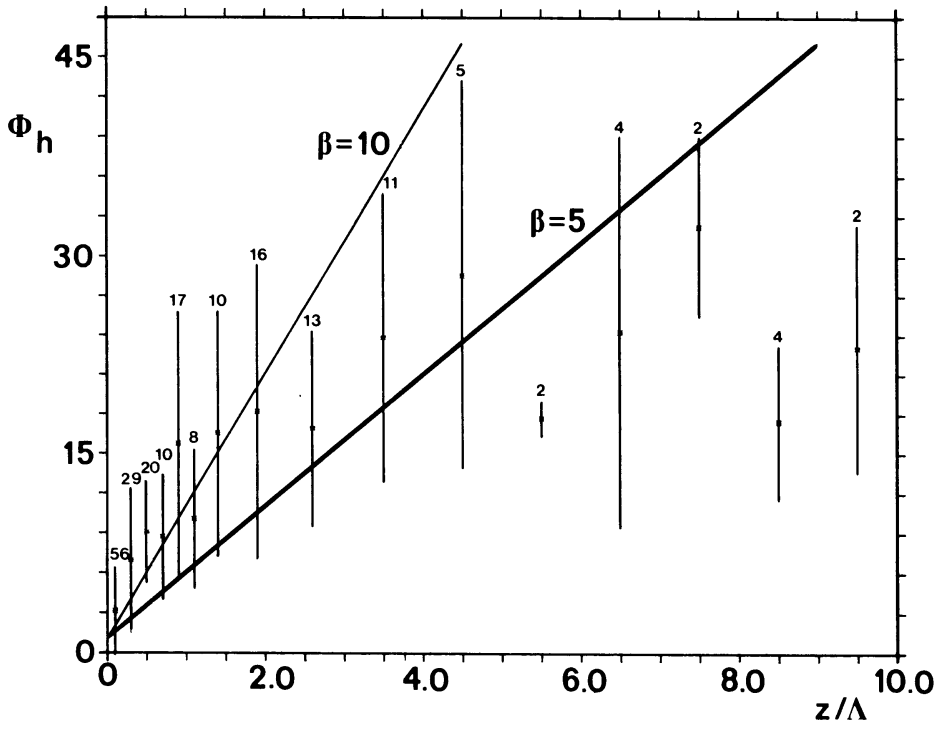

Fig.12b As Fig.12a, but now for the dimensionless temperature gradient Φ_h.

6. Conclusions

We examined the structure parameter of temperature in the stable, nocturnal boundary layer with continuous turbulence. The data were gathered during clear nights along the meteorological mast at Cabauw, The Netherlands.

The vertical profile of the temperature structure parameter depends on the geostrophic wind speed. In nights with a moderate geostrophic wind speed and in the first few hours of nights with a high geostrophic wind speed the structure parameter is large near the surface and decreases continuously to become small at the top of the boundary layer. In nights with a high geostrophic wind speed the observations show, a few hours after transition, the development of a maximum of the structure parameter at about three quarters of the boundary layer.

Comparing these observations with three theoretical profiles leads to the following conclusions:

Because of the assumptions of stationarity and constant Ri and Ri_f the model of Nieuwstadt (1985) is not suited to describe the profile of the structure parameter.

Using similarity functions following Sorbjan (1986) we found qualitative agreement between observations and model in the lower part of the boundary layer. Because the constants α_1 and α_2 in the stress and heat flux profiles could not be determined experimentally for each night apart we can not simulate the profiles in the rest of the boundary layer. However, calculations with assumed values of α_1 and α_2 show that the maximum at $z/h \approx 0.7$ observed at nights with a high geostrophic wind can not be explained. Like the model of Nieuwstadt, the model using similarity functions shows that the profile of CTN is a function of the stability parameter. The observations do not show such a dependency.

The model of Duynkerke and Driedonks shows the right shape of the profile in moderate and high geostrophic wind speed situations. However, the computed value of the structure parameter is 2-3 times higher than observed. This discrepancy may be a result of the difference in the observed and modelled dimensionless temperature and wind gradient functions in the surface layer. Observations at Cabauw show a relation of the form $1 + 10\ z/L$ rather than the in the literature generally accepted (and in the model used) relation $1 + 5\ z/L$.

References:

André, J.C., and L. Mahrt, 1982: The nocturnal surface inversion and influence of clear-air radiative cooling. J. Atmos. Sci., 39, 864-878.

Brost, R.A., and J.C. Wyngaard, 1978: A model study of the stably stratified planetary boundary layer. J. Atmos. Sci., 35, 1427-1440.

Businger, J.A., 1982: Equations and concepts, 1-36. In: F.T.M. Nieuwstadt and H. van Dop (eds.), Atmospheric turbulence and air pollution modelling, Reidel Publishing Company.

Caughey, S.J., J.C. Wyngaard and J.C. Kaimal, 1979: Turbulence in the evolving stable boundary layer. J. Atmos. Sci., 36, 1041-1052.

Corrsin, S., 1951: On the spectrum of isotropic temperature fluctuations in an isotropic turbulence. J. Appl. Phys., 22, 469-473.

Deardorf, J.W., 1978: Efficient prediction of ground surface temperature and moisture, with inclusion of a layer of vegetation. J. Geoph. Res., 83, 1889-1903.

Driedonks, A.G.M., and A.F. de Baas, 1983: Internal waves in the stably stratified atmospheric boundary layer. Preprints Sixth Symp. on Turbulence and Diffussion, Boston, Amer. Meteor. Soc., 276-279.

Duynkerke, P.G., and A.G.M. Driedonks, 1987: A model for the turbulent structure of the stratocumulus-topped atmospheric boundary layer. J. Atmos. Sci., 44, 43-64.

Dyer, A.J., 1974: A review of flux-profile relationships. Boundary-Layer Meteor., 7, 363-372.

Fairall, C.W., 1987: A top-down and bottom-up diffusion model of C_T^2 and C_Q^2 in the entraining convective boundary layer. J. Atmos. Sci., 44, 1009-1017.

Finnigan, J.J., and F. Einaudi, 1981: The interaction between an internal gravity wave and the planetary boundary layer, Part II: Effect of the wave on the turbulence structure. Quart. J. Roy. Meteor. Soc., 107, 807-832.

Kondo, J., O. Kanechika and N. Yasuda, 1978: Heat and momentum transfer and strong stability in the atmospheric surface layer. J. Atmos. Sci., 35, 1012-1021.

Lacser, A., and S.P.S. Arya, 1986: A numerical model study of the structure and similarity scaling of the nocturnal boundary layer. Boundary-Layer Meteor., 35, 369-385.

Monin, A.S., and A.M. Obukhov, 1954: Basic laws of turbulent mixing in the atmosphere near the ground. Tr. Akad. Nauk. SSSR, Geophiz. Inst., No.24 (151), 163-187.

Monna, W.A.A., and J.G. van der Vliet, 1987: Facilities for research and weather observations on the 213 m tower at Cabauw and at remote locations. Scientific reports WR-nr 87-5, KNMI, De Bilt, The Netherlands.

Nieuwstadt, F.T.M., 1984: The turbulent structure of the stable, nocturnal boundary layer. J. Atmos. Sci., 41, 2202-2216.

Nieuwstadt, F.T.M., 1985: A model for the stationary, stable boundary layer, 149-179. In: J.C.R. Hunt (ed.), Turbulence and diffusion in stable environments, Clarendon press, Oxford, England.

Sorbjan, Z., 1986: On similarity in the atmospheric boundary layer. Boundary-Layer Meteor., 34, 377-397.

Tatarski, V.I., 1961: Wave propagation in a turbulent medium (translated by R.A. Silverman), McGraw Hill, New York.

Wieringa, J., 1967: Evoluation and design of windvanes. J. Appl. Met., 6, 1114-1122.

Wieringa, J., 1972: Tilt errors and precipitation effects in trivane measurements of turbulent fluxes over water. Boundary-layer Meteor., 2, 406-426.

Wyngaard, J.C., and M.A. LeMone, 1980: Behaviour of the refractive index structure parameter in the entraining convective boundary layer. J. Atmos. Sci., 37, 1573-1585.

Yaglom, A.M., 1977: Comments on wind and temperature flux-profile relationships. Boundary-Layer Meteor., 11, 89-102.

Part II

Vertical profiles of the structure parameter of refractive index in the earth's atmosphere

1. Introduction

In clear nights stars can be seen to scintillate or twinkle, that is, their apparent brightness fluctuates rapidly. To the unaided eye scintillation appears as a brightness variation but in a telescope the intensity variations are less obvious than the variations in sharpness and position. The varying brightness of the stellar image makes observing more difficult and, at times, the accompanying spreading and jumping of the image is so severe that observations must be abandoned.

The intensity of scintillation decreases as the star rises above the horizon. This suggests that the effect is a function of the depth of the earth's atmosphere traversed by the incoming starlight. Scintillation is due to local fluctuations in the refractive index of air. For visible wavelengths the variation of refractive index depends only on air density and, therefore on air temperature, pressure and water-vapour pressure. Because the effects of the latter two are small in comparison with that of temperature the variation of refractive index is mainly due to small scale temperature fluctuations, caused by the turbulence of air. As the wavelength increases the refractive index of air ceases to be dependent on density only, and other factors are introduced that increase the effect of vapour pressure. At radio wavelengths this effect becomes important.

Wave propagation theory enables us to discern several parts in the atmosphere that have a clear influence on stellar image degradation (section 2). "Seeing" and the resolution of an optical system will also be discussed.

Information about the vertical profile of the structure parameter of refractive index is important to study which parts of the earth's atmosphere cause image degradation. In section 3 we will describe two methods to obtain these vertical profiles. Both methods are based on measuring temperature fluctuations. After determining the temperature structure parameter the structure parameter of refractive index can be calculated when temperature and pressure are known.

Using stellar scintillations the vertical profiles of the structure parameter of refractive index can be obtained as well. A technique that

uses a single star as a source and a spatially filtered detector as a receiver will be discussed in section 4.

In section 5 we will give some results of measurements of the vertical profile of the refractive index structure parameter. Measurements into the stratosphere are presented.

2. The effects of atmospheric turbulence on seeing

In wave propagation studies the turbulent atmosphere is often visualized as consisting of lenses (actually the eddies) of different scale sizes within the inertial subrange of spatial sizes, that is bounded by the inner (l_o) and outer (L_o) scale of turbulence. l_o is the size of the smallest eddies (in the order of a millimeter), that dissipate their kinetic energy into heat. L_o is the size of the largest atmospheric inhomogeneities for which atmospheric turbulence may still be considered isotropic. An electromagnetic wave propagating in a turbulent atmosphere exhibits random fluctuations of amplitude, phase and angle of arrival due to the refractive index fluctuations. As a consequence, an optical image formed by focusing such a wave exhibits fluctuations in intensity, sharpness and position, which is referred to as scintillation, image blurring, and image movement or quivering, respectively.

Consider a plane wave $u = A \exp(iS)$ with amplitude A and phase S, propagating through the turbulent atmosphere with refractive index N, which is only a function of position (Figure 1). The time-independent, scalar wave equation may be written as (Coulman, 1985):

$$\nabla^2 u + (\frac{2\pi}{\lambda})^2 N^2 u = 0. \qquad (2.1)$$

If the perturbations are small, we may find a solution of (2.1) in the form of an unperturbed wave u_o and a perturbation u', where $|u_o| >> |u'|$. The fluctuations of logarithmic-amplitude and phase may be expressed as:

$$\ln (A/A_o) = \chi , \qquad (2.2a)$$

$$S - S_o = S', \qquad (2.2b)$$

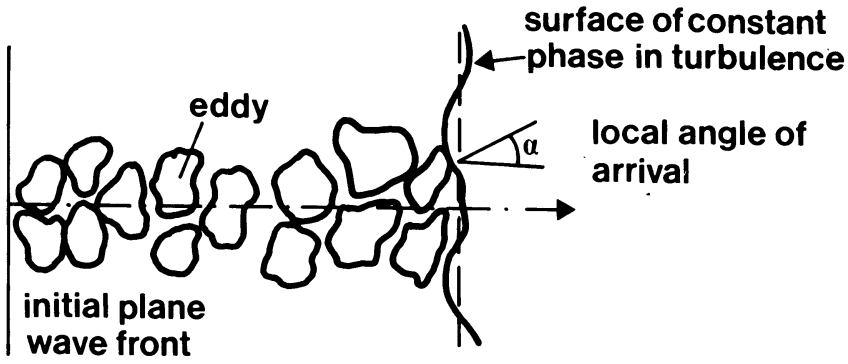

Fig.1 Schematic of a plane wave propagating through the turbulent atmosphere (from Brunner, 1982).

where A_o and S_o are the amplitude and phase of the unperturbed wave u_o.

The structure function $D_\Psi(r)$ for a variable Ψ is defined as (Part I, section 3):

$$D_\Psi(r) = \overline{[\Psi(r_1) - \Psi(r_2)]^2}, \tag{2.3}$$

where $r = r_1 - r_2$ is the separation between two points in the plane perpendicular to the propagation direction at the receiving plane ($l_o << r << L_o$).

The plane wave structure function $D_W(r)$ is defined as the algebraic sum of the structure functions for log-amplitude $D_A(r)$ and phase $D_S(r)$:

$$D_W(r) \equiv D_A(r) + D_S(r). \tag{2.4}$$

Assuming locally isotropic turbulence $D_W(r)$ can be derived as (Tatarski, 1971):

$$D_W(r) = 2.92\, r^{5/3} k^2 \sec\zeta \int_{z_T}^{z_m} C_N^2(z)\, dz, \tag{2.5}$$

where $k = \frac{2\pi}{\lambda}$ is the wavenumber, $C_N^2 = D_N(r) r^{-2/3}$ is the refractive

index structure parameter, ζ is the zenith angle, z_T is the height above the ground of the receiving telescope, and z_m the height at which $C_N^2 \rightarrow 0$. $C_N^2(z)$ is allowed to vary smoothly along the propagation path of the wave.

The variance of log-amplitude is given by:

$$\sigma_\chi^2 = 0.56\, k^{7/6} (\sec \zeta)^{11/6} \int_{z_T}^{z_m} z^{5/6} C_N^2(z)\, dz \,. \qquad (2.6)$$

The relation between σ_χ^2 and the structure function $D_A(r)$ is given by (Tatarski, 1961; see also Part I, section 3: σ_χ^2 equals $B_A(0)$):

$$\sigma_\chi^2 = B_A(0) = 1/2\, D_A(\infty). \qquad (2.7)$$

The "scintillation index" or the variance of relative intensity fluctuations σ_I^2 equals $4\,\sigma_\chi^2$. From (2.6) follows that inhomogeneities which are farthest away from the observation point have the greatest effect on the intensity fluctuations.

The structure function of phase $D_S(r)$ can be calculated with sufficient accuracy from the following relationships (Brunner, 1982):

$$D_S(r) \approx \begin{Bmatrix} 0.5 \\ 1.0 \end{Bmatrix} D_W(r), \quad \begin{matrix} l_o << r << R \\ L_o > r >> R \end{matrix} \,, \qquad (2.8)$$

where R is the radius of the first Fresnel zone:

$$R = (\lambda L)^{1/2} \,, \qquad (2.9)$$

with L the length of the propagation path $z_m - z_T$ ($R \approx 10 - 30$ cm). With (2.5) and (2.8) we see that all inhomogeneities, regardless of their distance from the observation point, have the same effect on the phase fluctuations.

Image movement and image blurring are caused by fluctuations in the tilt of the mean wave front (angle of arrival fluctuations) and corrugation of the mean wave front, respectively, at the receiving aperture of a telescope. For a telescope with aperture diameter d the variance of the angle of arrival fluctuations is given by (Tatarski, 1971):

$$\sigma_\alpha^2 = \frac{D_S(d)}{k^2 d^2} \quad . \tag{2.10}$$

Substituting the formulae for $D_S(r)$ into (2.10) yield:

$$\sigma_\alpha^2 \approx \begin{Bmatrix} 1.46 \\ 2.92 \end{Bmatrix} d^{-1/3} \sec\zeta \int_{z_T}^{z_m} C_N^2(z)\, dz, \quad \begin{matrix} l_o \ll d \ll R \\ L_o > d \gg R \end{matrix} \quad . \tag{2.11}$$

The variance of the angle of arrival fluctuations σ_α^2 depends on aperture diameter d and the strength of atmospheric turbulence. However, σ_α^2 is not directly dependent on the wavenumber k of the radiation.

Phase inhomogeneities with scales smaller than d cause blurring of the stellar image and exist even in an instantaneous observation. Phase inhomogeneities with scales larger than d cause the movements of clear images. However, by using short exposures, i.e. exposure times < 0.01 s (Fried, 1966), the effect of the fluctuations of the tilt of the mean wave front can be removed. Short-exposure images are clear and do not move.

The lateral coherence length r_o is used as a measure of atmospheric "seeing". r_o is related to $D_W(r)$ by (Brunner, 1982):

$$r_o = 3.18\, r\, [D_W(r)]^{-3/5}, \tag{2.12a}$$

or with (2.5) given by:

$$r_o = 0.184\, [\lambda^2 / \int_{z_T}^{z_m} C_N^2(z)\, dz]^{3/5} \quad . \tag{2.12b}$$

For $d < r_o$ the resolution δ of the optical system depends in the usual manner on the aperture diameter:

$$\delta = 1.22\, \lambda/d \approx 12".6/\, d\ (\text{cm}), \tag{2.13}$$

for $\lambda = 0.5\ \mu m$. δ is the angular separation of two images that can just be resolved, and it is often called the diffraction limit. For $d > r_o$ the average resolution of the optical system is limited by r_o. An increase in d beyond r_o will not result in an improvement of the resolution of the optical system, considering a case with a certain

strength of atmospheric turbulence and long exposures. Pollaine et al. (1979) define "seeing" through a turbulent atmosphere as:

$$\text{Seeing} = \lambda / r_o. \tag{2.14a}$$

Substituting (2.12b) for r_o yields:

$$\text{Seeing} = 3.76\ k^{1/5}\ (\int_{z_T}^{z_m} C_N^2(z)\ dz)^{3/5} \tag{2.14b}$$

Seeing should improve for longer wavelengths, in proportion to the 1/5 power of λ.

3. Turbulence data collection

For optical wavelengths the variation of refractive index is mainly due to small scale temperature fluctuations. There is a simple relation between the structure parameter of refractive index C_N^2 and that of temperature C_T^2 (Gossard, 1977):

$$C_N^2(z) = [\frac{8P(z)}{T^2(z)} * 10^{-5}]^2 * C_T^2(z), \tag{3.1}$$

where P(z) is the pressure (millibars), T(z) is the air temperature (K) and z is the height. The result includes empirical constants and applies for wavelength of 0.5 μm.

Balloon-borne radiosondes can be used to determine the temperature structure parameter (Barletti et al., 1974; Bufton et al., 1972; Bufton, 1973). The radiosondes are equipped with two thermal sensors of platinum wire. The sensors are mounted in a horizontal plane 1 m apart.

Assuming isotropy and homogeneity of turbulence there is a relation between the temperature difference between two points and the structure parameter of temperature:

$$C_T^2 = \overline{[T(r_1) - T(r_2)]^2} \ / \ r^{2/3}, \tag{3.2}$$

where $r = |r_1 - r_2|$. This relation is valid only for distances r within

the inertial subrange. The distance r = 1 m fulfills at least theoretically (Hufnagel, 1966) this condition up to a great height above the tropopause.

The arm with the two thermal sensors is maintained perpendicular to any air flow by means of a back fin. The complete thermal sensor system is attached to the balloon with a 300 - 400 m nylon cord in order to minimize balloon-wake effects on the measurement of temperature fluctuations during the ascend of the balloon. The mean square temperature difference data (over a 5 sec averaging time) are sent by a radiosonde telemetry link to a ground receiver. The balloon ascends at 5 m/s and the payload descends by parachute at 10 m/s. The error of the C_T^2 measurement is estimated to be less than ± 10% of the reported values.

Standard meteorological radiosondes launched within a short period before or after the experiments and from a site close to the experiments provide the vertical profiles of temperature, pressure, relative humidity, wind speed and wind direction.

Another method to determine the vertical profile of the temperature structure parameter is by means of a level-flying aircraft (Pinus, 1985). Measurements of air-temperature fluctuations are made with fluctuation resistance thermometers. In order to obtain the true values of the temperature fluctuations θ' the readings θ'_r of the fluctuation thermometer must be corrected for dynamic heating and variations of altitude during level flight:

$$\theta' = \theta'_r - \beta U u' + \gamma \Delta H, \qquad (3.3)$$

where β is a coefficient, experimentally determined to be 0.83, U is the average speed of the aircraft with respect to the air, u' is the velocity fluctuation measured synchronously by the aircraft's thermo-anemometer and corrected for the influence of temperature fluctuations, γ is the lapse rate, and ΔH are the variations of flight altitude determined with a statoscope. With these high-frequency fluctuations measurements the dissipation of turbulent kinetic energy ε and the dissipation of temperature variance N can be determined. By applying the frozen-turbulence hypothesis ε and N are given by:

$$\varepsilon = 15\ \nu\ \overline{\left(\frac{\partial u'}{\partial x}\right)^2} = \frac{15\nu}{U^2}\ \overline{\left(\frac{\partial u'}{\partial t}\right)^2}\ , \qquad (3.4a)$$

$$N = 6\gamma\ \overline{\left(\frac{\partial \theta'}{\partial x}\right)^2} = \frac{6\gamma}{U^2}\ \overline{\left(\frac{\partial \theta'}{\partial t}\right)^2}\ , \qquad (3.4b)$$

where ν is the kinematic viscosity and γ the molecular diffusivity for temperature (Champagne et al., 1977). The temperature structure parameter can be determined with:

$$C_T^2 = 3.2\ \varepsilon^{-1/3}\ N. \qquad (3.5)$$

Relation (3.1) is used to calculate C_N^2 from these aircraft data and pressure and temperature at the same height.

4. Scintillation data collection

Stellar scintillations, induced by atmospheric turbulence, are a problem to astronomical observations. However, observations of the twinkling stars and the motion of stellar images yield information about the turbulence and the wind speed in the upper atmosphere.

Vertical profiles of the structure parameter of refractive index can be derived from stellar scintillation measurements (Ochs et al., 1976). The spatial structure of the stellar scintillation pattern is viewed through filters that pass only a narrow band of spatial frequencies. By running many such signals through filters of different spatial wavelength and combining the outputs with appropriate weights a set of reasonably sharp-peaked path-weighting functions centered at different heights can be obtained.

Assume that the star irradiance I, perturbed by atmospheric turbulence and received on the ground, can be decomposed into a fluctuating part I' and a mean irradiance $\bar{I}$. When stellar scintillations are observed near the zenith they are sufficiently weak to permit the use of the first-order scattering theory of Tatarski (1961). Then the covariance of the unfiltered irradiance scintillation normalized to the mean irradiance is given by:

$$C_I(x' - x'') = \langle I'(x')\, I'(x'') \rangle / \bar{I}^2 =$$

$$0.528\, \pi^2\, k^2 \int_0^\infty dz\, C_N^2(z) \int_0^\infty dK\, K^{-8/3} \sin^2 [K^2 z/(2k)]$$

$$* J_o [K(x' - x'')] , \qquad (4.1)$$

where $k = 2\pi/\lambda$, λ is the wavelength of the incident starlight, K is a two-dimensional spatial wavenumber, and J_o is a Bessel function of the first kind of order zero. Assuming statistical homogeneity of I in the receiving plane the variance of the normalized filtered intensity scintillation is defined by:

$$\sigma_I^2 = D^{-2} \int_{-D/2}^{D/2} dx' \int_{-D/2}^{D/2} dx'' \cos(2\pi x'/d) \cos(2\pi x''/d)\, C_I(x'-x''), \qquad (4.2)$$

when a one-dimensional sinusoidal spatial filter of length D and wavelength d is used.

After substituting (4.1) into (4.2) and performing the integrations σ_I^2 can be written in the form of a weighting function (Ochs et al., 1976):

$$\sigma_I^2 = \int_0^\infty dz\, C_N^2(z)\, W(z), \qquad (4.3)$$

where the path-weighting function is given by:

$$W(z) = 0.264\, \pi\, k^2 \int dK \left\{ \frac{\sin[\frac{1}{2} D\,(K-K_o)]}{\frac{1}{2} D\,(K-K_o)} + \frac{\sin[\frac{1}{2} D\,(K+K_o)]}{\frac{1}{2} D\,(K+K_o)} \right\}^2$$

$$* K^{-8/3}\, W_o(\tfrac{z}{2k} K^2), \qquad (4.4)$$

$K_o = \frac{2\pi}{d}$, and W_o is the weighting function for $D \to \infty$ (Figure 2a).

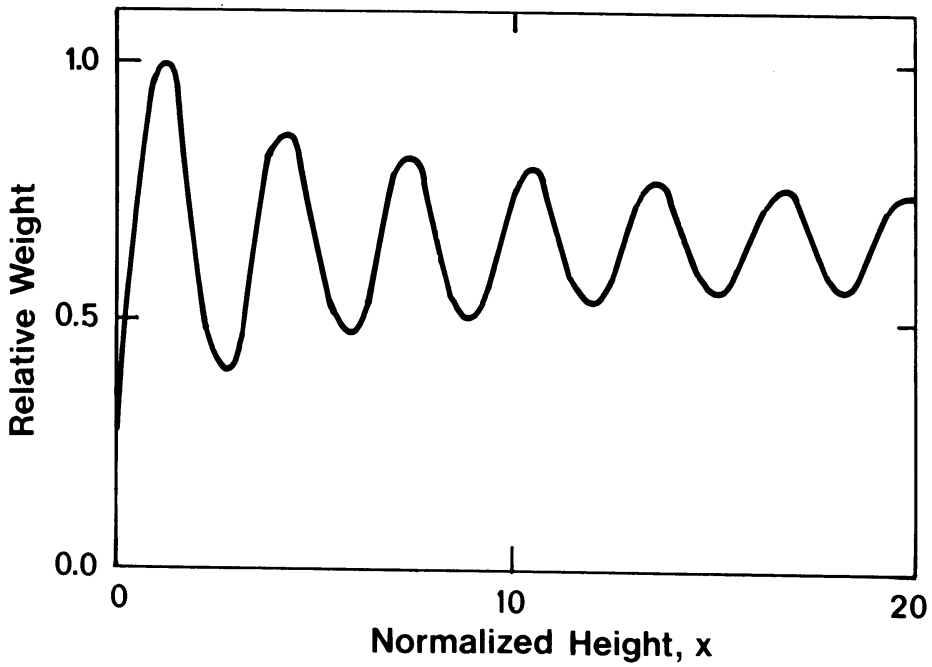

Fig.2a Weighting function of an infinite linear array of detectors observing the scintillations of a monochromatic plane wave source. The relative weight is shown as a function of normalized height $x = \pi z\lambda/d^2$, where z is the height of the turbulence and d is the spatial wavelength of the array of detectors (from Ochs et al., 1976).

Because a star is not emitting light at a single wavelength, the path-weighting function must be averaged over the bandwidth of the detected signal, which is mainly limited by the response of the photomultiplier tube (Figure 2b). The oscillation seen in Figure 2a is smeared out because of the broadband effect. It can also be seen that for smaller spatial wavelengths d there is more contribution from the lower atmosphere, whereas for larger d higher parts of the atmosphere become more important.

To measure the vertical profile of turbulence the height resolution of these weighting functions are too poor. However, by combining several path-weighting functions with appropriate relative weights a set of

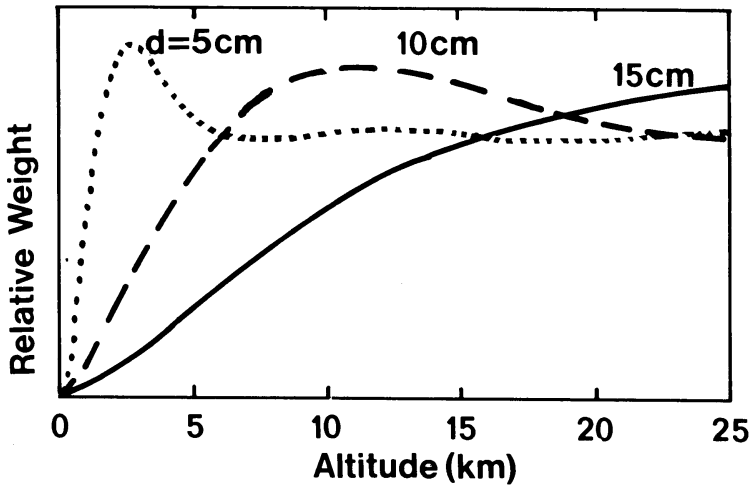

Fig.2b Weighting function of a finite linear array of detectors (array length = 35.6 cm) observing stellar scintillations for various spatial wavelength d. The finite bandwidth of the light source has been included (from Ochs et al., 1976).

reasonably sharp-peaked path-weighting functions centered at different heights can be obtained (Figure 3). Ochs et al. (1976) used the composite path-weighting function given by:

$$W_c(z) = \sum_{i=1}^{3} R_i \, K_i^{8/3} \, W'(z, d_i), \qquad (4.5)$$

where R_i is the relative weight given to the i^{th} spatial wavenumber $K_i = 2\pi/d_i$, and d_i is the i^{th} spatial wavelength. $W'(z, d_i)$ is the path-weighting function corrected for the finite bandwidth of the light source. The peak altitude, the three spatial wavelengths d_i needed for each lineair combination, and the relative weights R_2 and R_3 ($R_1 = 1$) are shown in Table 1.

With the path-weighting function $W_c(z)$ the structure parameter of refractive index C_N^2 of each measurement can be expressed as:

Tabel 1. The Peak Altitudes and Relative Inverse Areas (see Eq. (4.6b)) of Each of the Seven Weighting Functions W_i shown in Fig. 3.

	W_1	W_2	W_3	W_4	W_5	W_6	W_7
Peak altitude (km)	2.25	3.75	5.25	7.5	9.75	12.75	> 14.5
B x 10^{14}	2.39	1.91	2.57	1.84	1.38	1.46	0.87
d_1 (cm)[a]	5	6.5	7	8.5	10	11.5	14
d_2 (cm)	8	9	5	6	6.5	7.5	9
d_3 (cm)	15	15	11	13	15	15	7
R_2	-0.65	-0.6	-0.38	-0.35	-0.27	-0.24	-0.73
R_3	-0.33	-0.36	-0.53	-0.56	-0.66	-0.67	+0.23

[a] The d_i are the spatial wavelengths that must be combined to produce each W, the relative weights being R_2 and R_3 ($R_1 \equiv 1$). (From Ochs et al., 1976)

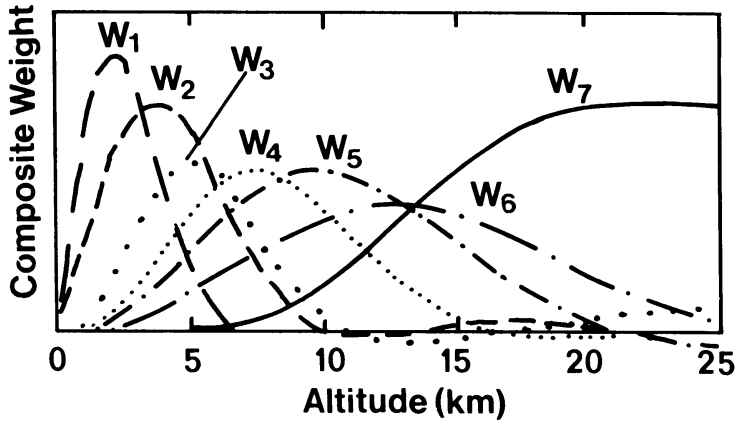

Fig.3 Composite path-weighting functions obtained by linearly combining weighting functions at three different spatial wavelengths. See text and Table 1 for details (from Ochs et al., 1976).

$$C_N^2 = B \sum_{i=1}^{3} R_i K_i^{8/3} \sigma_I^2 (d_i), \qquad (4.6a)$$

where

$$B = 1.87 * 10^{-13} \left[\int_0^\infty dz\, W_c(z) \right]^{-1}. \qquad (4.6b)$$

The calibration factor B is obtained by measuring the areas under the curves shown in Figure 3 (for W_7 this is done upto 25 km). $\sigma_I^2 (d_i)$ is the normalized irradiance variance detected by a one-dimensional spatial filter with spatial wavelength d_i.

5. Observations of the vertical profile C_N^2

From section 2 it is clear that knowledge of $C_N^2(z)$ is required in order to estimate the effects of atmospheric turbulence on seeing. The vertical profile of C_N^2 has been measured by balloon-borne radiosondes (e.g., Barletti et al., 1974; Bufton et al., 1972; Bufton, 1973), level-

flying aircrafts (Pinus, 1985) and one-dimensional spatial filtering of scintillations (Ochs et al., 1976). In this section we will discuss a number of these measurements. We will restrict ourselves to night-time observations at visible wavelengths.

In Figure 4 the results of the ascending part of a balloon flight on June 29, 1973 over the island of Tenerife (Canary Islands) are shown (Barletti et al., 1974). There is a strong surface turbulence in the first 100-200 m above the ground (2400 m above mean sea level, MSL) with C_N^2 values of the order of 10^{-15} $m^{-2/3}$, after which the turbulence quickly decreases. Turbulence in the middle part of the troposphere is layered with layer thicknesses between 100 and 500 m. The turbulence is low and decreases with height from 10^{-17} $m^{-2/3}$ to 10^{-18} $m^{-2/3}$.

From data obtained on three balloon flights at dawn during September 1971 in southeastern New Mexico Bufton et al. (1972) found large values of C_N^2 ($2-3 * 10^{-16}$ $m^{-2/3}$) in the first 100 m above the surface (1.2 km

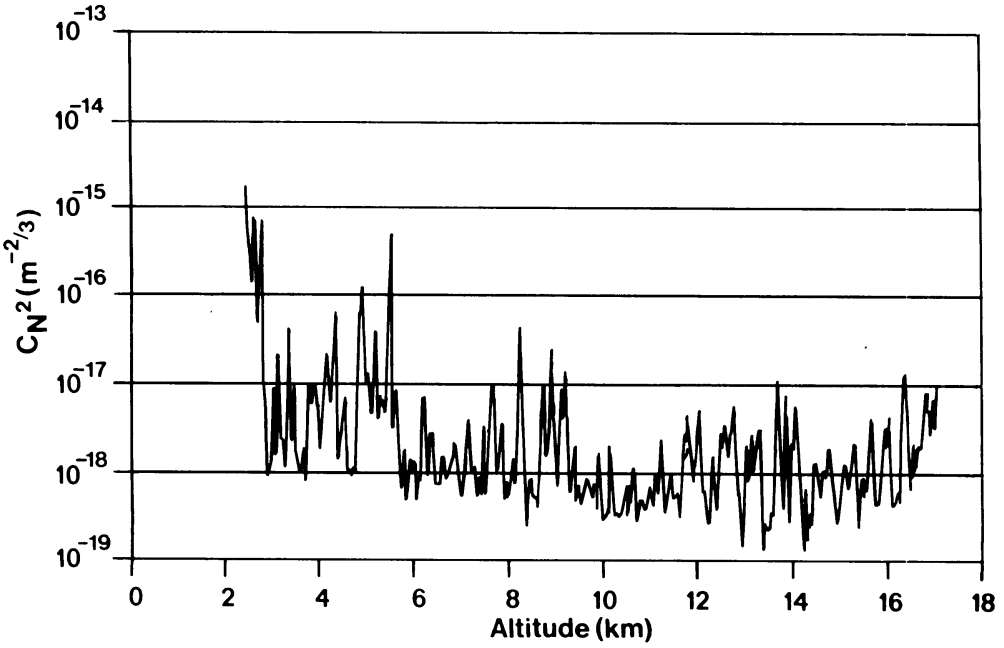

Fig.4 Refractive index structure parameter C_N^2 ($m^{-2/3}$) versus altitude z (km) for a balloon flight on June 29, 1973, 2000 LT (after sunset). (From Barletti, 1974.)

above MSL) and a relatively rapid decrease to a minimum near 3 km (MSL). This is followed by an increase of C_N^2 to a maximum, which may be associated with mountain-lee waves (there are mountains 50 km to the west and 20 km to the east with summits 2-3 km above MSL). Then there is a gradual decrease to a longer stretch of minimum values ($5 * 10^{-18}$ $m^{-2/3}$) in the 7-9 km (MSL) region. Above 9 km (MSL), the mean value of C_N^2 decreases more slowly or even becomes constant. Throughout the troposphere layers with typical thicknesses of 100-200 m are observed. Near the tropopause (15-16 km above MSL) an increased spiking and layer activity is seen with thin layers of strength $1-5 * 10^{-17}$ $m^{-2/3}$.

Figure 5 shows examples of C_N^2, temperature and wind speed profiles recorded on August 10, 1972 with a balloon flight near Beltsville, Maryland (Bufton, 1973). Values of C_N^2 at ground level (50 m above MSL) were about $4.5 * 10^{-14}$ $m^{-2/3}$. The most dominant C_N^2 structures above the surface layer were layers associated with the temperature inversions at 2.4 km and 4.8 km and with the tropopause region (13-14 km above MSL).

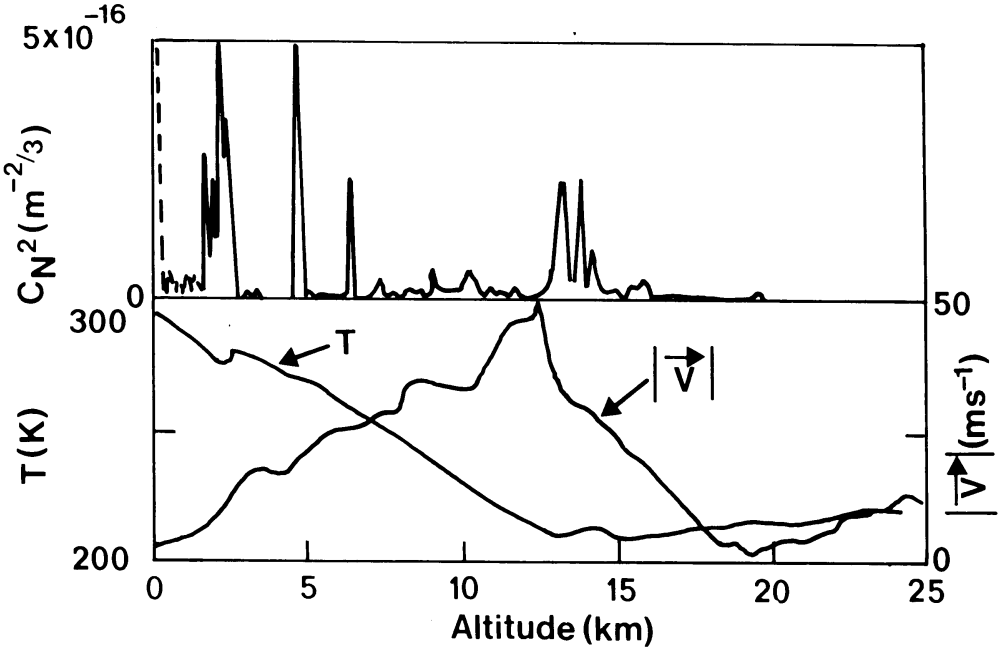

Fig.5 Refractive index structure parameter C_N^2, temperature T and wind speed |V| versus altitude z above mean sea level for a flight on August 10, 1972 (from Bufton, 1973).

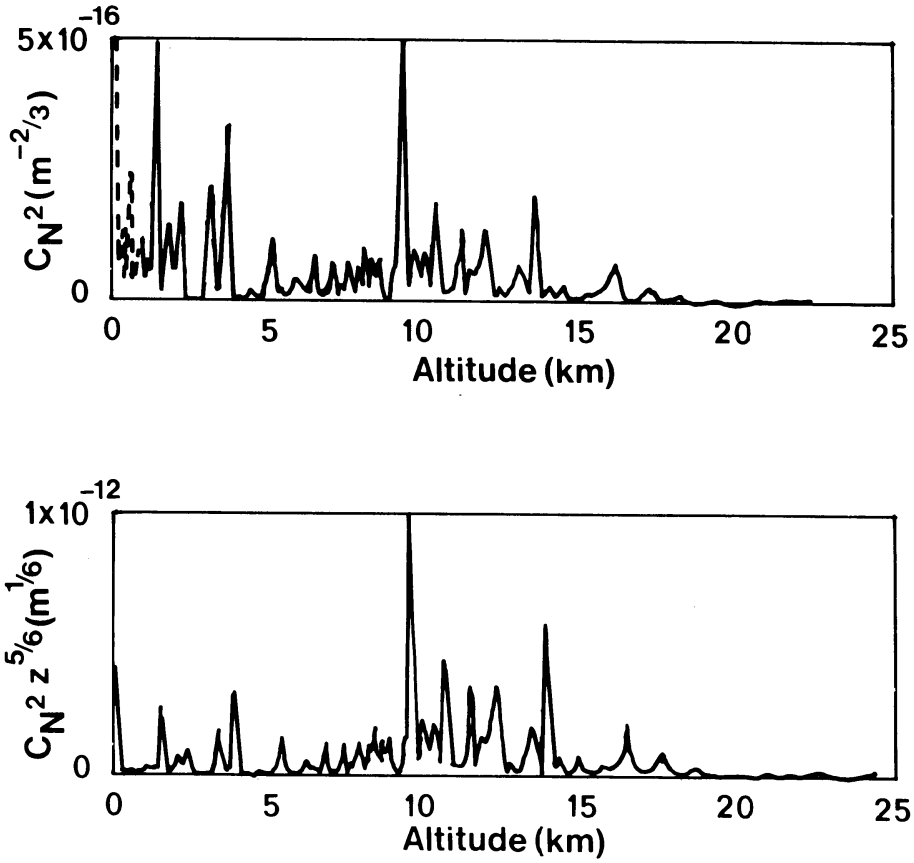

Fig.6 The profiles of the observed C_N^2 (top) and the calculated values of $C_N^2 z^{5/6}$ (bottom) versus altitude z above mean sea level for a balloon flight on September 6, 1972 (from Bufton, 1973).

The profiles of C_N^2 and $C_N^2 z^{5/6}$, based on a balloon flight on September 6, 1972, are shown in Figure 6. Bufton computed that the contribution to

$$\int_0^{h_{max}} C_N^2(z)\, dz \approx 1.8 * 10^{-12}\ m^{1/3}$$

from the surface layer (first 10 m) was about 47%, whereas the contribution to

$$\int_0^{h_{max}} C_N^2(z)\, z^{5/6}\, dz \approx 1.6 * 10^{-9}\ m^{7/6}$$

from the profile below 9 km was 28% (h_{max} = 24.1 km). Thus, although the surface layer contributes dominantly to the integral of C_N^2(seeing), its effect on the amplitude fluctuations (scintillation) is small. The height resolution that can be achieved with balloon-borne radiosonde measurements is about 25-50 m.

In Figure 7 we show some results obtained by Ochs et al. (1976) at Boulder, Colorado using the stellar scintillation measurement technique described in section 4. The height resolution with this technique is much less. However, again we see large values of C_N^2 near the surface (1700 m above MSL). The profile of 25 June shows a continuous decrease of C_N^2 with height. The profiles of 3 July and 16 September decrease rapidly from the surface to about 5 km (MSL), then increase to a maximum at 10 km (MSL), after which they decrease again. The increase of C_N^2 might be associated with mountain-wave effects, caused by the Rocky Mountains (with tops of 4000 m), some 20 km to the west of the measurement location. These curves are averages of measurements on a single evening. There are large night to night variations of the

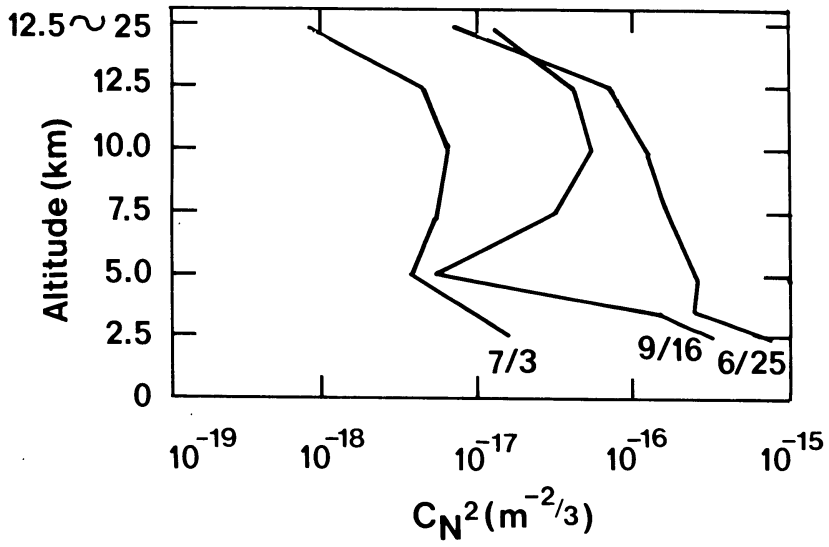

Fig.7 Typical optically measured vertical C_N^2 profiles at Boulder, Colorado. Each curve is the average of the measurements of a single evening (from Ochs et al., 1976).

vertical C_N^2 profile. The typical variation over a period of 2½ h in a single evening is shown in Figure 8. Within a couple of hours there are noticeable changes.

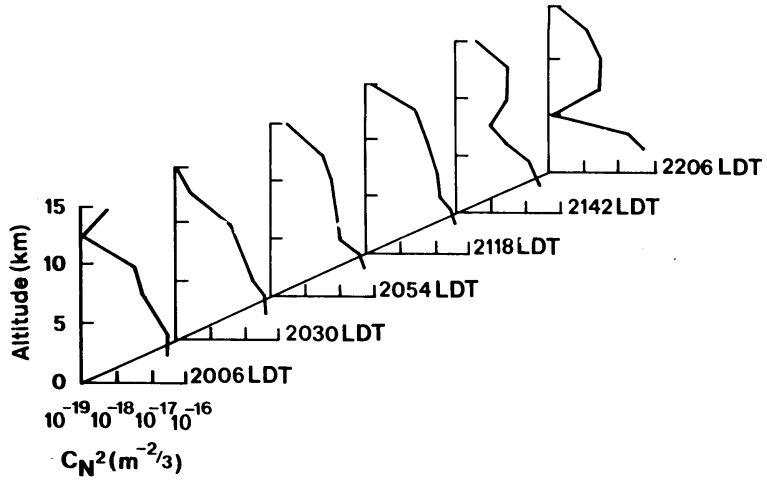

Fig.8 Typical variation of the vertical C_N^2 profile in a single evening (from Ochs et al., 1976).

The profiles discussed so far are mostly profiles up to the tropopause (13-16 km above MSL). They show an increase of C_N^2 near the tropopause. The profile obtained by Bufton (Figure 5) shows that C_N^2 is again small above the tropopause with some structure well into the stratosphere up to 17 km.

Barat and Bertin (1984) show results of a sounding performed on 28 April 1978 with a high-resolution balloon-borne instrument in the stably stratified stratosphere. Between 25.5 and 27.5 km they measured the turbulent small-scale thermal fluctuations within seven turbulent layers with thicknesses varying between 10 and 250 m (Figure 9). When we use eq. (3.1), the observed pressure and a typical value for the temperature in that part of the stratosphere ($T \approx 220$ K) we can calculate the structure parameter of refractive index (Table 2). It follows that these values of C_N^2 in the stratosphere are at least an order of magnitude

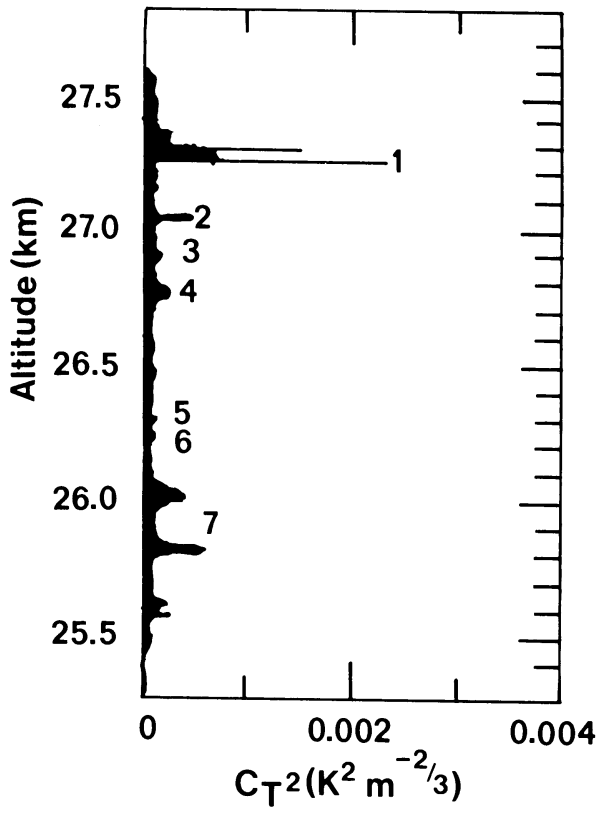

Fig.9 Vertical profile of the structure parameter C_T^2 between 25.5 and 27.5 km (from Barat and Bertin, 1984).

Table 2 The structure parameter of refractive-index in the stratosphere

Layer	Pressure (mb)	C_T^2 ($K^2 m^{-2/3}$)	C_N^2 ($m^{-2/3}$)
1	18	$2.3 * 10^{-3}$	$2.0 * 10^{-18}$
2	19	$0.4 * 10^{-3}$	$3.9 * 10^{-19}$
4	20	$0.2 * 10^{-3}$	$2.2 * 10^{-19}$
7	22	$0.3 * 10^{-3}$	$4.0 * 10^{-19}$

less than values commonly observed in the troposphere.

Pollaine et al. (1979) measured a nighttime value of

$$\int C_N^2 \, dz \approx 4 * 10^{-12} \, m^{1/3}$$

at Mt. Wilson Observatory. Bufton (1973) computed several integrals from the C_N^2 profiles obtained near Beltsville, Maryland, with a mean value of

$$\int C_N^2 \, dz = 1.5 * 10^{-12} \, m^{1/3}.$$

The lateral coherence length r_o can now be calculated using (2.12b) and $\lambda = 0.5$ μm. We find $r_o = 3.5$ cm and 6.3 cm, respectively. At Maui Observatory, Miller and Zieske (1977) have used the spatial frequency modulation of stellar images to estimate that at $\lambda = 0.5$ μm, the early-morning (0100-0500) value of r_o lies between 5.3 and 17.8 cm, with a mean value of 9.6 cm.

With these values and eq. (2.14a) the seeing at $\lambda = 0.5$ μm lies between 3" (Mt. Wilson obs.) and 0.6" (best value at Maui Observatory).

6. Conclusions

Based on the results discussed here and on profiles shown by others (e.g., Fante, 1980; Gossard, 1977) we come to the following conclusions about the vertical profile of the structure parameter of refractive index:

C_N^2 is large near the ground with values varying between 10^{-14} $m^{-2/3}$ and 10^{-16} $m^{-2/3}$. C_N^2 varies from position to position and from time to time. On the meteorological mast at Cabauw we found that at 20 m C_N^2 varies between 10^{-14} $m^{-2/3}$ and 10^{-15} $m^{-2/3}$.

Above the boundary layer there generally is a sharp decrease of C_N^2 . In the troposphere turbulence is clearly layered with typical thicknesses of 100-500 m. Values of the order of 10^{-17}-10^{-18} $m^{-2/3}$ are found for C_N^2. However, an increase of C_N^2 is seen in situations with winds from or towards mountains. The increase starts at about the same height as the height of the mountain tops. A few kilometers higher C_N^2 decreases again. This effect is still noticeable when the mountains are a few tens of kilometers away from the observation spot. Temperature inversions in the troposphere also cause an increase of C_N^2.

After an increase of C_N^2 in the tropopause region ($\sim 10^{-17}$ $m^{-2/3}$) the structure parameter becomes small in the stratosphere ($C_N^2 \sim 10^{-19}$ $m^{-2/3}$).

With these vertical profiles of C_N^2 and the computations of Bufton (1973) it seems reasonable to expect the lower troposphere to be most responsible for phase fluctuations (see eq. (2.11)) causing image movement and image blurring, whereas the tropopause region seems to be more responsible for amplitude fluctuations (see eq. (2.6)) causing scintillation.

At different locations and times the lateral coherence length r_o varies between 3.5 and 17.8 cm. Because astronomical telescopes have apertures d much larger than r_o the average resolution of the optical system is limited by r_o. For long exposures the resolution equals the seeing disk, that was found to vary between 0.6" and 3".

References:

Barat, J., and F. Bertin, 1984: Simultaneous measurements of temperature and velocity fluctuations within clear air turbulence layers: analysis of the estimate of dissipation rate by remote sensing techniques. J. Atmos. Sci., 41, 1613-1619.

Barletti, R., G. Ceppatelli, E. Moroder, L. Paternò and A. Righini, 1974: A vertical profile of turbulence in the Atlantic air mass measured by balloon-borne radiosondes. J. Geophys. Res., 79, 4545-4549.

Brunner, F.K., 1982 : The effects of atmospheric turbulence on telescopic observations. Bull. Geod., 56, 341-355.

Bufton, J.L., 1973: Comparison of vertical profile turbulence structure with stellar observations. Appl. Opt., 12, 1785-1793.

Bufton, J.L., P.O. Minott, M.W. Fitzmaurice, and P.J. Titterton, 1972: Measurements of turbulence profiles in the troposphere. J. Opt. Soc. Am., 62, 1068-1070.

Champagne, F.H., C.A. Friehe, J.C. LaRue, and J.C. Wyngaard, 1977: Flux measurements, flux estimation techniques, and fine-scale turbulence measurements in the unstable surface layer over land. J. Atmos. Sci., 34, 515-530.

Coulman, C.E., 1985: Fundamental and applied aspects of astronomical "seeing". Ann. Rev. Astron. Astrophys., 23, 19-57.

Fante, R.L., 1980: Electromagnetic beam propagation in turbulent media: an update. Proc. IEEE, 68, 1424-1443.

Fried, D.L., 1966: Optical resolution through a randomly inhomogeneous medium for very long and very short exposures. J. Opt. Soc. Am., 56, 1372-1379.

Gossard, E.E., 1977: Refractive index variance and its height distribution in different air masses. Radio Sci., 12, 89-105.

Hufnagel, R.E., 1966: Restoration of atmospherically degraded images, appendix 3, vol.2, Nat. Acad. Sci., Washington, D.C.

Miller, M., and P. Zieske, 1977: Measurement of the atmospheric correlation scale. J. Opt. Soc. Am., 67, 1680-1685.

Ochs, G.R., Ting-i Wang, R.S. Lawrence, and S.F. Clifford, 1976: Refractive-turbulence profiles measured by one-dimensional spatial filtering of scintillations. Appl. Opt., 15, 2504-2510.

Pinus, N.Z., 1985: Brief communications: Vertical profiles of the refractive-index structure parameter in the troposphere and stratosphere. Atmos. Oceanic Phys., 21, 64-67.

Pollaine, S., A. Buffington, and F.S. Crawford, 1979: Measurement of the size of the isoplanatic patch using a phase-correcting telescope. J. Opt. Soc. Am., 69, 84-89.

Tatarski, V.I., 1961: Wave propagation in a turbulent medium (translated by R.A. Silverman), McGraw-Hill, New York.

Tatarski, V.I., 1971: The effects of the turbulent atmosphere on wave propagation, (Translated from the Russian), Keter Press, Jerusalem.